Smart Nanocomposites

Volume 3, Number 1

Table of Contents

nova publishers
New York

Smart Nanocomposites

This Journal presents new studies in the fast growing area of smart materials, in particular, composite nanostructured materials. It focuses on the physics and physical chemistry of surfaces, interfaces, thin films and coatings, nanoparticles and other nanostructures, as well as on their new and smart applications. Original approaches in fabrication and applications of nanostructured materials will get special attention. Nanostructured ceramics, alloys, various nanocarbon forms (nanotubes, fullerenes, graphene) and their composites used in sensors (including single molecule sensing) and actuators, artificial metabolism, drug delivery, selective membranes, fuel cells, energy storage, and photovoltaics are just a few examples of new classes of materials and applications that are within the scope of the Journal. It features the results of interdisciplinary research from universities, national labs, and privately owned companies.

The Journal is peer-reviewed with the highest standards and quality of publications. The purpose of this Journal is to bring the most up-to-date advances in nanotechnology together, and to give research groups the opportunity to compare their results with other groups' data. To achieve this, the Journal focuses mostly on practical applications of nanodevices, and on proof of the concept publications. Areas of interest include (but not are limited to): sensors, smart membranes, smart coatings for corrosion protection, aspects of significance to nanorobots: power supplies, nanorobot manipulating devices, and microchips for artificial intelligence. The Journal also deals with safety issues: safety of nanotechnology to the environment, controlling the nanodevices, and other aspects.

Smart Nanocomposites
is published in two issues per year by

Nova Science Publishers, Inc.
400 Oser Avenue, Suite 1600
Hauppauge, New York 11788-3619, U.S.A.
Telephone: (631) 231-7269, Fax: (631) 231-8175
E-mail: nova.main@novapublishers.com
Web: www.novapublishers.com

ISSN: 1949-4823

Subscription Rate per Volume (2012)
Print: $245 Electronic: $245 Combined Print + Electronic: $367

Additional color graphics might be available in the e-version of this journal.

Smart Nanocomposites
Volume 3, Number 1
ISSN: 1949-4823

SYNTHESIS AND CHARACTERIZATION OF SOME SCHIFF BASES METAL COMPLEXES AND THEIR INVESTIGATION AS ANTIBACTERIAL AND ANTIFUNGAL AGENTS

Ahmed M. A. El-Seidy*

Inorganic Chemistry Department, National Research Center,
Cairo, Egypt.
Chemistry Department, Faculty of Science, The Imam Muhammad bin
Saud Islamic University, Riyadh, Saudi Arabia.

ABSTRACT

New series of Fe(III), Co(II), Cu(II) and Ni(II) of the 6,6'-((1E,1'E)-(propane-1,2-diylbis(azanylylidene))bis(methanylylidene))bis(7-hydroxy-5-methoxy-2-methyl-4H-chromen-4-one), H_2L, have been synthesized and characterized by elemental analysis, IR, UV-vis, ^{1}H-NMR, mass and ESR spectra, magnetic susceptibility and molar conductivity measurements. The spectral data and magnetic measurements of the complexes indicate that, the geometries are either square planar or octahedral. The antibacterial and antifungal activities of the compounds showed that, some of metal complexes exhibited a greater inhibitory effect than standard drug as tetracycline (bacteria), Amphotericin B (fungi), the parent ligand and the corresponding metal ion.

Keywords: Schiff base ligand, Biological activity, antibacterial, antifungal, metal complexes

INTRODUCTION

Schiff base ligands played an important role in the development of coordination chemistry and they have been employed throughout the transition metal series. Metal complexes of these ligands are characterized by their facile synthesis, the accessibility of diverse structural modifications and the availability of chiral versions. [1, 2] Transition metal complexes with oxygen and nitrogen donor Schiff bases are of particular interest [3] because of their ability to possess unusual configurations, be structurally labile and their sensitivity to molecular environments. [4] Schiff base ligands have proven to be very effective in constructing supramolecular architectures such as coordination polymers, double helixes, and

* Corresponding authors at: Inorganic Chemistry Department, National Research Centre, Dokki, 12622, Cairo, Egypt. Tel.: 002-01095105802. E-mail address: ahmedmaee2@gmail.com.

triple helicates. [5] Schiff bases can accommodate different metal centres involving various coordination modes allowing successful synthesis of homo- and heterometallic complexes with varied stereochemistry. This feature is employed for modelling active sites in biological systems. [6, 7] Additionally, they have wide applications in fields such as antibacterial, antiviral, antifungal agents, [8] homogeneous or heterogeneous catalysis [9, 10] and magnetism. [11] Schiff bases are potential anticancer drugs and when administered as their metal complexes, the anticancer activity of these complexes is enhanced in comparison to the free ligand. [12]

In view of the versatile importance of Schiff bases and their complexes, I report in this article the synthesis and characterization of the ligand 6,6'-((1E,1'E)-(propane-1,2-diylbis(azanylylidene))bis(methanylylidene))bis(7-hydroxy-5-methoxy-2-methyl-4H-chromen-4-one), H_2L and its Fe(III), Co(II), Cu(II) and Ni(II) complexes. The coordination behavior of the Schiff base ligand towards metal ions was investigated via IR, UV-Vis, ESR as well as conductivity and magnetic moments measurements. The antibacterial and antifungal activities of the compounds showed that, some of metal complexes exhibited a greater inhibitory effect than standard drug as tetracycline (bacteria) and amphotericin B (fungi).

EXPERIMENTAL

1.1. Material

All the reagents employed for the preparation of the ligand and its complexes were of the best grade available and used without further purification.

1.2. Synthesis of the Schiff base ligand H_2L

Ethanol solution (5 mL) of propane-1,2-diamine (1.1 mmole, 7.9 X 10^{-2} g) was added to a hot 70^{o}C ethanol solution (15 mL) of 6-acetyl-7-hydroxy-5-methoxy-2-methyl-4H-chromen-4-one (2.1 mmole, 0.5 g) and reflux for 4h then the solvent was evaporated to 10 mL. After coaling the yellow precipitate was filtered off and dried under vacuum over anhydrous $CaCl_2$, Scheme 1. ^{1}H NMR (300MHz, $CHCl_3$): δ =12.08 [S, 1H, H(22)], 11.53 [S, broad, H(37)], 8.97 [S, 2H, H(46) and H(41)], 5.77 [m, 2H, H(44) and H(42)], 5.66 [S, 2H, H(45) and H(43)], 4.04 [psd, 2H, H(39) and H(38)], 3.51[S, 6H, C$\underline{H}_3$(36) and C$\underline{H}_3$(21)], 3.43 [m, 1H, H (40)], 2.21 [S, 3H, C$\underline{H}_3$(34)], 2.19[S, 3H, C$\underline{H}_3$(19)], 1.40 [d, 3H, C$\underline{H}_3$(3)], Scheme 2.

1.3. Synthesis of the Metal Complexes

1.3.1. Preparation of Complexes 5, 7 and 9:

A hot (60° C) methanol solution of the copper chloride or copper acetate was added to a hot (60° C) 1,1-dichloroethane solution of the ligand with molecular ratios 1:1 L/M (ligand /metal) (complex **5**) and 2:1 L/M (complexes **7** and **9**). Complex **5** was obtained in case of using copper chloride or copper acetate. The reaction mixture was then refluxed for a 4 h. The

precipitates formed were filtered, washed with ethanol, then with diethyl ether and dried under vacuum over anhydrous $CaCl_2$.

1.3.2. Preparation of Other Complexes

Other metal complexes of the ligand H_2L were prepared by mixing a hot (60° C) methanol solution of the metal salts with the required amount of a hot (75° C) ethanol solution of the ligand to form 1:1 or 1:2 L/M (ligand /metal). The reaction mixture was then refluxed for a time depending on the transition metal salt used. The precipitates formed were filtered, washed with ethanol, then with diethyl ether and dried under vacuum over anhydrous $CaCl_2$.

1.3.3. In-Vitro Antibacterial and Antifungal Activities

The investigation of the biological activities of the newly synthesized Schiff base ligand, its metal complexes and their corresponding metal salts were carried out in the Botany Department Lab. of microbiology, Faculty of Science, El-Menoufia University. The antibacterial and antifungal activities were investigated by disc diffusion method. [13] The antibacterial activities were done using *Escherichia coli* and *Aspergillus niger*. The tested compounds were dissolved in DMSO to give 2000 ppm stock solutions. DMSO poured disc was used as negative control. The bacteria were subcultured in nutrient agar medium which was prepared using ($g.L^{-1}$ distilled water) NaCl (5 g), peptone (5 g), beef extract (3 g), agar (20 g). The fungus was subcultured in Dox´s medium which was prepared using ($g.L^{-1}$ distilled water) yeast extract (1g), sucrose (30 g), $NaNO_3$, agar (20 g), KCl (0.5 g), KH_2PO_4 (1 g), $MgSO_4.7H_2O$ (0.5 g) and trace of $FeCl_3.6H_2O$. These mediums were then sterilized by autoclaving at 120 ^{0}C for 15 min. After cooling to 45 ^{0}C the medium was poured into 90 mm diameter Petri dishes and incubated at 37 ^{0}C or 28 ^{0}C, respectively. After few hours, Petri dishes were stored at 4 ^{0}C. Microorganisms were spread over each dish by using sterile bent Loop rod. The test is carried out by placing filter paper disks with a known concentration of the compounds on the surface of agar plates inoculated with a test organism. Standard antibacterial drug (tetracycline), antifungal drug (Amphotericin B) and solution of metal salts were also screened under similar conditions for comparison. The Petri dishes were incubated for 48 h. at 37 or 28ºC, respectively. The zone of inhibition was measured in millimeters carefully. All determinations were made in duplicated manner for all compounds. The average of the two independent readings was record.

1.4. Physical Measurements

The ligand and its metal complexes were analyzed for C, H, N, Cl and M contents at the Microanalytical Laboratory, Faculty of Science, Cairo University, Egypt. Analytical and physical data of the ligand H_2L and its metal complexes are reported in Table 1. The metal ion contents of the complexes were also determined by the previously reported methods. [14-16] IR spectra of the ligand and its metal complexes were measured using KBr discs with a Jasco FT/IR 300E Fourier transform infrared spectrophotometer covering the range 400–4000 cm^{-1} and in the 500–100 cm^{-1} region using polyethylene-sandwiched Nujol mulls on a Perkin Elmer FT-IR 1650 spectrophotometer. ^{1}H NMR spectra was obtained on 300 MHz VARIAN NMR spectrometers. Chemical shifts (ppm) are reported relative to TMS. The mass spectra were run at 70 eV with HP MODEL: MS. 5988A. The electronic spectra of the ligand and its complexes were obtained in Nujol mulls using a Shimadzu UV–240 UV–Vis recording

spectrophotometer. Molar conductivities of the metal complexes in DMSO (10^{-3} M) were measured using a dip cell and a Bibby conductimeter MC1 at room temperature. The resistance measured in ohms and the molar conductivities were calculated according to the equation: $\Lambda = V \times K \times Mw/g \times \Omega$, where Λ, molar conductivity (ohm^{-1} cm^2 mol^{-1}); *V*, volume of the complex solution (mL); *K*, cell constant 0.92 cm^{-1}; *Mw*, molecular weight of the complex; *g*, weight of the complex; and Ω, resistance measured in ohms. Magnetic moments at 298 K were determined using the Gouy method with $Hg[Co(SCN)_4]$ as calibrant. The solid ESR spectra of the complexes were recorded with ELEXSYS E500 Brucker spectrometer in 3-mm Pyrex Tubes at 298 K. Diphenylpicrylhydrazide (DPPH) was used as a g-marker for the calibration of the spectra.

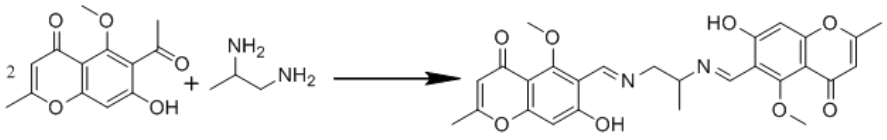

Scheme 1. Schematic representation for the formation of the ligand H_2L.

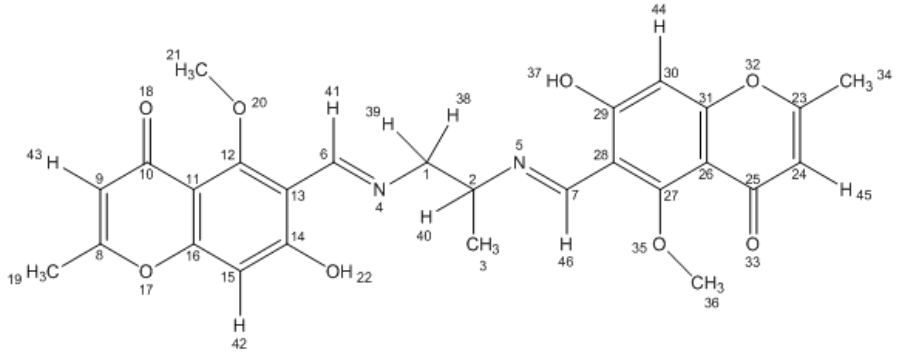

Scheme 2. Numbering scheme employed for H_2L (**1**).

RESULTS AND DISCUSSION

Elemental Analysis

The elemental and physical data of the ligand H_2L and its complexes (Table 1) showed that the stoichiometry of the complexes obtained is either 1:1 or 2:1 M/L (metal:ligand).

Mass Spectra of the Ligand

The mass spectra of the Schiff base ligand H_2L revealed the molecular ion peak at m/e 506, which is coincident with the formula weight (506.5) for this ligand and supports the identity of the structure.

Infrared Spectra

The important spectral bands of the synthesized ligand as well as the complexes are presented in Tables 2. The Schiff base ligand exhibit two broad bands centered at 3250 and 3247 cm^{-1} due to *ν*(O–H). These bands disappeared on complexation with the metal ion in case of complexes 3, 5, 11 and 12, which indicates the deprotonation of the ligands prior to coordination through oxygen atom. [17, 18] In other complexes these bands were shifted to lower wave number (10-20 and 12-22 cm^{-1}) with decreasing their intensities indicating their coordination to the metal ion. [18-20] A strong bands around 1648 and 1651s cm^{-1} due to azomethine group of the ligand undergoes shifted to lower wave number (18-26 and 15-23 cm^{-1}) with decreasing their intensities indicating the coordination to the azomethine nitrogen to metal ion. [18, 21, 22] The band at 1218 cm^{-1} in the free ligand may be assigned to the phenolic C–O stretching. [23] In the complexes, C–O stretching vibrations are shifted to higher frequency by 7-24 cm^{-1}. This shift to higher frequency indicates the bonding of phenolic oxygen to metal ion. [24] The strong band at 1663 and 1661 cm^{-1} due to carbonyl groups of the ligand almost showed no shift in all complexes indicating that both carbonyl groups were not involved in complexation.

Some complexes included water molecules. The broad bands in the 3485-3441 cm^{-1} region are due to coordinated water or water of crystallization. The bands for water of crystallization are different from those of coordinated water. The presence of water molecules within the coordination sphere in the hydrated complexes 3, 6, 8, 10, 12 and 13 is supported by the presence of bands in the 3432-3448 , 1600-1610, 940-955 and 620-632 cm^{-1} regions due to OH stretching, HOH deformation, H_2O rocking and H_2O wagging, respectively. [25] The absence of coordinated water molecules in complexes 2, 4 and 11 was confirmed from the absence of the rocking, twisting and wagging vibrational modes which are normally activated in 970-930 cm^{-1} and 660-600 cm^{-1} regions, [26] as well as the presence of weak and broad bands in 3530-3485 cm^{-1} range indicating that the water in all of these complexes is lattice rather than coordinated. [27]

Extensive IR spectral studies reported on metal aceto complexes indicate that the acetate ligand may coordinate to a metal center in either a monodentate, bidentate or bridging manner. [27] The $\nu_{asym.}(CO_2)$ and $\nu_{sym.}(CO_2)$ of the free acetate ions are at 1560 cm^{-1} and 1416 cm^{-1}, respectively. [27] In monodcntate coordination ν(C=O) is found at higher energy than $\nu_{asym.}(CO_2)$ and ν(C-O) is lower than $\nu_{sym.}(CO_2)$. As a result, the separation between the two ν(CO) bands is much larger in monodentate complexes than the free ion as found for the complex 4, 9 and 10 [22, 28] and this is supported by the appearance of two new bands in 1579-1593 and 1363-1384 cm^{-1} regions, which may be attributed to ν_{asym} (COO^-) and $\nu_{sym.}(COO^-)$, respectively. The separation value (Δ) between ν_{asym} (COO^-) and $\nu_{sym.}(COO^-)$ in these complexes was more than 200 cm^{-1} (209-216) suggesting the coordination of carboxylate group in a monodentate fashion. [28, 29] Further, the complex exhibits δ(COO) at 750 cm^{-1} which is considered diagnostic for unidentate acetates. [30] The opposite trend is observed in bidentate aceto coordination; the separation between ν(CO) is smaller than for the free ion. For bridging acetate with both oxygens coordinated as in copper(ll) acetate, however, the two ν(CO) bands are close to the free ion values. [22, 29, 31, 32]

The spectra of the complexes 2-3, 5-8 and 12-13 showed two assignable, weak intensity ν (M-CI) bands in 410-377 cm^{-1} range indicating terminal Chloro ligands. [33]

Conductivity Measurements

All metal complexes are stable in air and insoluble in common organic solvents but easily soluble in DMF and DMSO. The molar conductivities of the complexes in DMF (10^{-3} M) are listed in table 1. All complexes show a non-electrolyte nature. [22, 32, 34]

Electronic Spectra and Magnetic Moments

The solid state spectrum of the ligand H_2L shows a broad band at 268 nm assignable to the phenyl ring $\pi\rightarrow\pi^*$ transitions [35, 36] and 355 nm assignable to $\pi\rightarrow\pi^*$ of C=N groups. [37]

The $n\rightarrow\pi^*$ transition associated with the (C=N) moiety found around 395 nm in the spectrum of the free ligand and is generally shifted to higher energy on complexation. [38] There are also charge-transfer transitions partially responsible for the intense colors of the complexes. The bands present at energies above 333 nm in the spectra of the metal complexes are Cl→ M(II) and O→ M(II) bands. [35, 36]

The cobalt(II) complexes 2 and 6 have spectra typical of an octahedral system showing two bands, in 622-639 and 467-480 nm regions, assignable to $^4T_{1g}$ (F) → $^4A_{2g}$ (F) (ν_2) and $^4T_{1g}$ (F)→$^4T_{2g}$ (P) (ν_3) transition, respectively, indicating an octahedral structure. [39-41] The magnetic moment value (μ_{eff}) of the Co(II) complex 2 found to be 4.7 B. M., which lie in the range reported for high spin (S = 3/2) octahedral cobalt(II) complexes. [42]

Complexes 3 and 12 showed two bands in 490-495 and 645-655 nm regions which are assignable to $^6A_{1g} \rightarrow {}^4A_{1g}(G)$ and $^6A_{1g} \rightarrow {}^4T_{2g}(G)$ transitions, respectively, suggesting its octahedral nature. [41, 43]

The magnetic moment of complex 3 is 5.5 BM which is closer to the spin only value indicating an octahedral structure for the complex. [44]

The nickel(ll) complex 13 have electronic spectra typical of an octahedral system showing two bands lie at 645 and 510 nm which may be assigned to $^3A_{2g}\rightarrow {}^3T_{1g}(F)$ (ν_2) and $^3A_{2g}\rightarrow {}^3T_{1g}(P)$ (ν_3) transitions, respectively, in an octahedral geometry. [45-47] The diamagnetic complex 11 showed shoulder at 539 nm characteristic of a square planar diamagnetic Ni(II) complexes, [48] and resemble the absorption bands observed in the spectrum of an analogous Ni(II) complexes reported by Bouwman [49].

Copper complexes 4, 8 and 10 showed signals in 567-580 and 622-635 nm regions, which were assigned to $^2B_1\rightarrow{}^2E$ and $^2B_1\rightarrow{}^2B_2$ transitions indicating a distorted octahedral structure, [50] while complexes 5, 7 and 9 complexes register a broad band in 540-543 nm region due to $^2B_{1g} \rightarrow {}^2E_g$ transition in a square planar Cu(II) structure [51].

The magnetic moment of complex 4 is 1.82 B.M. indicating the presence of one unpaired electron. The electronic spectral results clearly indicated square planar geometry for the Cu(II) system, which should contain one unpaired electron, where μ_{eff} value would be in the range 1.8–2.1 B.M. [52].

The magnetic moment of complexes 6-10 and 12-13 were smaller than the calculated value for two metal ions and this may be due to antiferromagnetism between the two ion-centers. [22, 32, 53] The structure representation of metal complexes is present in figure 1.

Table 1. Analytical and physical data of the ligand H_2L and its metal complexes

No.	Ligand/ Complexes	FW	Yield (%)	Analysis (%) / Found (calcd)					Molar Conductance
				C	H	N	Cl	M	
1	H_2L $C_{27}H_{26}N_2O_8$	506.5	71	63.8(64.0)	5.4(5.2)	5.6(5.5)	-	-	-
2	$[H_2LCoCl_2].2H_2O$ $C_{27}H_{30}Cl_2CoN_2O_{10}$	672.4	65	48.0(48.2)	5.6(4.5)	4.5(4.2)	10.2(10.6)	8.7(8.8)	21
3	$LFeCl.H_2O$ $C_{27}H_{26}ClFeN_2O_9$	613.8	73	52.5(52.8)	4.4(4.3)	4.8(4.6)	5.7(5.8)	9.0(9.1)	18
4	$[H_2LCu(OC(O)CH_3)_2].3H_2O$ $C_{31}H_{38}CuN_2O_{15}$	742.2	81	50.0(50.2)	5.3(5.2)	4.1(3.8)	-	8.4(8.6)	13
5	LCu $C_{27}H_{24}CuN_2O_8$	568.0	79	57.0(57.1)	4.6(4.3)	5.0(4.9)	-	11.0(11.2)	7
6	$H_2LCo_2Cl_4(H_2O)_4$ $C_{27}H_{34}Cl_4Co_2N_2O_{12}$	838.2	74	38.6(38.7)	4.1(4.1)	3.6(3.3)	16.8(16.9)	14.0(14.1)	25
7	$H_2LCu_2Cl_4$ $C_{27}H_{26}Cl_4Cu_2N_2O_8$	775.4	84	41.5(41.8)	3.6(3.4)	3.8(3.6)	18.2(18.3)	16.2(16.4)	20
8	$H_2LCu_2Cl_4(H_2O)_4$ $C_{27}H_{34}Cl_4Cu_2N_2O_{12}$	847.5	79	38.1(38.3)	40.1(4.0)	3.6(3.3)	16.5(16.7)	14.9(15.0)	22
9	$H_2LCu_2(OC(O)CH_3)_4$ $C_{35}H_{38}Cu_2N_2O_{16}$	869.8	85	48.0(48.3)	4.5(4.4)	3.4(3.2)	-	14.5(14.6)	16
10	$H_2LCu_2(OC(O)CH_3)_4(H_2O)_4$ $C_{35}H_{46}Cu_2N_2O_{20}$	941.8	84	44.5(44.6)	5.1(4.9)	3.1(3.0)	-	13.2(13.5)	14
11	$[LNi].H_2O$ $C_{27}H_{26}N_2NiO_9$	581.2	88	55.6(55.8)	4.7(4.5)	5.0(4.8)	-	9.9(10.1)	8
12	$LFe_2Cl_4(H_2O)_4$ $C_{27}H_{32}Cl_4Fe_2N_2O_{12}$	830.1	69	39.0(39.1)	4.0(3.9)	3.6(3.4)	16.9(17.1)	13.4(13.5)	27
13	$H_2LNi_2Cl_4(H_2O)_4$ $C_{27}H_{34}Cl_4N_2Ni_2O_{12}$	837.8	73	38.5(38.7)	4.3(4.1)	3.4(3.3)	16.8(16.9)	13.8(14.0)	22

Molar Conductance $=\Lambda_m$ ($\Omega^{-1}cm^2mol^{-1}$).

Table 2. IR frequencies of the bands (cm-1) of ligand H_2L and its complexes and their assignments

No.	Ligand/ Complexes	ν(H_2O)	ν(OH)	ν(C=O)	ν(C=N)	ν(C–O)	ν_s(Coo), ν_{as}(Coo), (Δ)	ν(M-N)	ν(M-O)	ν(M-Cl)
1	H_2L	-	3250m, 3247m	1663s, 1661s	1648s, 1651s	1218m	-	-	-	-
2	$[H_2LCoCl_2].2H_2O$	3465b	3230m 3225sh	1662m	1631m	1225m	-	450m	410m	377
3	$LFeCl.H_2O$	3432b	-	1661m	1633m	1239m	-	495m	390m	398
4	$[H_2LCu(OC(O)CH_3)_2].3H_2O$	3485b	3236m 3225m	1663m	1628m	1228m	1579, 1363, 216	440w	400w	-
5	LCu	-	-	1660m	1625s	1241m	-	480m	380w	-
6	$H_2LCo_2Cl_4(H_2O)_4$	3445b	3235m, 3228m	1664m	1630m	1223m	-	460w	355w	405
7	$H_2LCu_2Cl_4$	-	3234m, 3230sh	1663m	1629m	1227m	-	450w	350w	375
8	$H_2LCu_2Cl_4(H_2O)_4$	3438b	3234m 3228m	1662m	1633m, 1627m	1224m	-	434m	364m	410
9	$H_2LCu_2(OC(O)CH_3)_4$	-	3240m 3230m	1660m	1628m	1229m	1586, 1376, 210	448m	394m	-
10	$H_2LCu_2(OC(O)CH_3)_4(H_2O)_4$	3448b	3240m 3235m	1663m	1630	1228m	1593, 1384, 209	445m	368m	-
11	$[LNi].H_2O$	3530b	-	1662b	1631m 1628sh	1242m	-	475m	355m	-
12	$LFe_2Cl_4(H_2O)_4$	-	3238m 3228m	1660b	1629m	1225m	-	441w	387m	400
13	$H_2LNi_2Cl_4(H_2O)_4$	3444b	3239m 3227m	1663b	1630	1227m	-	437m	380m	405

m=medium, s=strong, b=broad, w=week, sh=shoulder.

Table 3. The electronic absorption spectral bands (nm) and magnetic moment (B.M) for the ligand H_2L and its Metal complexes

No.	Ligand/ Complexes	π–π*, n–π*, and CT bands	d–d bands	μ_{eff} in BM
1	H_2L	268, 325, 395	-	-
2	$[H_2LCoCl_2].2H_2O$	278, 345, 390, 410	480, 639	4.7
3	$LFeCl.H_2O$	260, 366, 387, 407	490, 655	5.5
4	$[H_2LCu(OC(O)CH_3)_2].3H_2O$	268, 355, 392, 425	580, 635	1.71
5	LCu	255, 340, 380, 405	540	1.82
6	$H_2LCo_2Cl_4(H_2O)_4$	310, 335, 385, 410	467, 622	3.4
7	$H_2LCu_2Cl_4$	261, 342, 397, 400	541	1.53
8	$H_2LCu_2Cl_4(H_2O)_4$	299, 354, 396, 408	576, 630	1.49
9	$H_2LCu_2(OC(O)CH_3)_4$	288, 349, 397, 412	543	1.48
10	$H_2LCu_2(OC(O)CH_3)_4(H_2O)_4$	259, 355, 380, 422	574, 530	1.56
11	$[LNi].H_2O$	266, 345, 392, 402	539sh	-
12	$LFe_2Cl_4(H_2O)_4$	258, 364, 390, 413	495, 645	3.2
13	$H_2LNi_2Cl_4(H_2O)_4$	267, 355, 381, 400	510, 645	1.9

ESR Spectra

The ESR spectra of polycrystalline samples of copper(II) complexes (4-5 and 7-10) at room temperatures (298 K) were of axial shape with $g_{//} > g_{\perp}$ characteristic of complexes with $^2B_{1(dx2-y2)}$ orbital ground state. [54] The average g values were calculated according to the equation: $g_{av} = 1/3[g_{//} + 2\ g_{\perp}]$, Table 4. The complexes show $g_{\|}>g_{\perp}>g_e$, indicating a d_{x2-y2} ground state, and spectral features were characteristic of axial symmetry. [55] All complexes exhibit $g_{//} < 2.3$, suggesting covalent characters around the copper in present complexes. Kivelson and Neiman [56] have reported that a $g_{//}$ value greater than 2.3 indicates ionic character. The g-values were related by the expression, [22, 53] $G = (g_{\|}-2)/(g_{\perp}-2)$, if $G > 4.0$ then local tetragonal axes were aligned parallel or only a slightly misaligned, if $G < 4.0$, significant exchange coupling is present, table 4. Only complexes 4 and 5 showed $G > 4.0$ indicate that there is no direct copper-copper interaction in the solid state of these complexes. In case of other copper complexes, the G value is <4, which suggests considerable exchange interaction in these solid complexes. These complexes showed a half field signal, observed at 1600 G due to the $\Delta m_s = +2$ transitions, proving the Cu-Cu interaction but the absence of such signal in case of complexes 4 and 5 rules out any Cu-Cu interaction in these tow complexes. [57] The $g_{//}/A_{//}$ is taken as an indication for the stereochemistry of the copper(II) complexes. Addison [58] has suggested that this ratio may be an empirical indication of the tetrahedral distortion of the square planar geometry. The values of $g_{//}/A_{//}$ quotient in the range

105–135 cm^{-1} are expected for copper complexes within perfectly square based geometry and those higher than 150 cm^{-1} for tetrahedrally distorted complexes. The values of $g_{//}/A_{//}$ for complexes 5, 7 and 9 lie in the range 126-130 indicating a square planar geometry while the value for complexes 4, 8 and 10 lie in the range 195-214 indicating an octahedral geometry around copper ion.

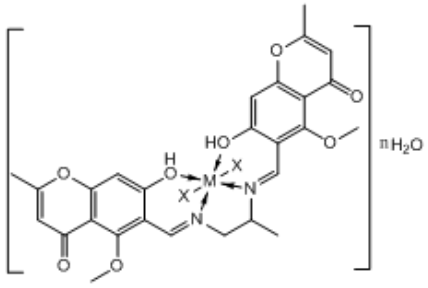

Complex **2**: $[H_2LCoCl_2].2H_2O$, M=Co, X=Cl, n=2
Complex **4**: $[H_2LCu(OC(O)CH_3)_2].3H_2O$, M=Cu, X=$OC(O)CH_3$, n=3

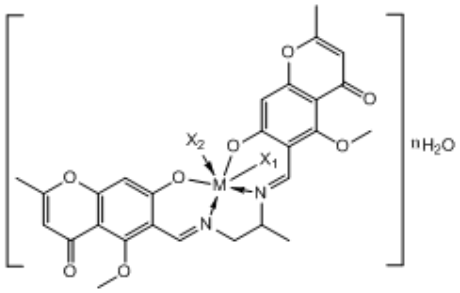

Complex **3**: $LFeCl.H_2O$, M=Fe, X_1=Cl, X_2=H_2O, n=none
Complex **5**: LCu, M=Cu, X_1=X_2=None, n=none
Complex **11**: $[LNi].H_2O$, M=Ni, X_1=X_2=none, n=1

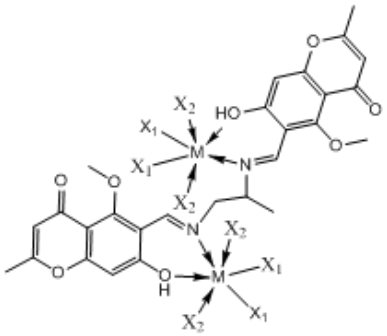

Complex **6**: $H_2LCo_2Cl_4(H_2O)_4$, M=Co, X_1=Cl, X_2=H_2O
Complex **7**: $H_2LCu_2Cl_4$, M=Cu, X_1=Cl, X_2=none
Complex **8**: $H_2LCu_2Cl_4(H_2O)_4$, M=Cu, X_1=Cl, X_2=H_2O
Complex **9**: $H_2LCu_2(OC(O)CH_3)_4$, M=Cu, X_1=$OC(O)CH_3$, X_2=none
Complex **10**: $H_2LCu_2(OC(O)CH_3)_4(H_2O)_4$, M=Cu, X_1=($OC(O)CH_3$), X_2=H_2O
Complex **13**: $H_2LNi_2Cl_4(H_2O)_4$, M=Ni, X_1=Cl, X_2=H_2O

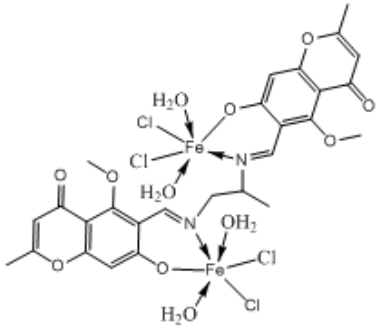

Complex **12**: $LFe_2Cl_4(H_2O)_4$

Figure 1. The proposed structures of metal complexes of the ligand H_2L

Table 4. ESR parameters for copper(II) complexes

No.	Complexes	$g_{//}$	$g_{\perp}$	$g_{//}/A_{//}$	G	$g_{av.}$
4	$[H_2LCu(OC(O)CH_3)_2].3H_2O$	2.22	2.040	195	5.5	2.10
5	LCu	2.15	2.030	130	5.0	2.07
7	$H_2LCu_2Cl_4$	2.10	2.037	127	2.7	2.10
8	$H_2LCu_2Cl_4(H_2O)_4$	2.15	2.040	214	3.8	2.13
9	$H_2LCu_2(OC(O)CH_3)_4$	2.09	2.029	126	3.1	2.09
10	$H_2LCu_2(OC(O)CH_3)_4(H_2O)_4$	2.14	2.039	204	3.6	2.10

Biological Activity

The results of biological activity tested for ligands and their complexes are given in figures 2, 3. Diameter of inhibition zone (mm) including the disc diameter was measured for each treatment. The ligands showed no activity at all.

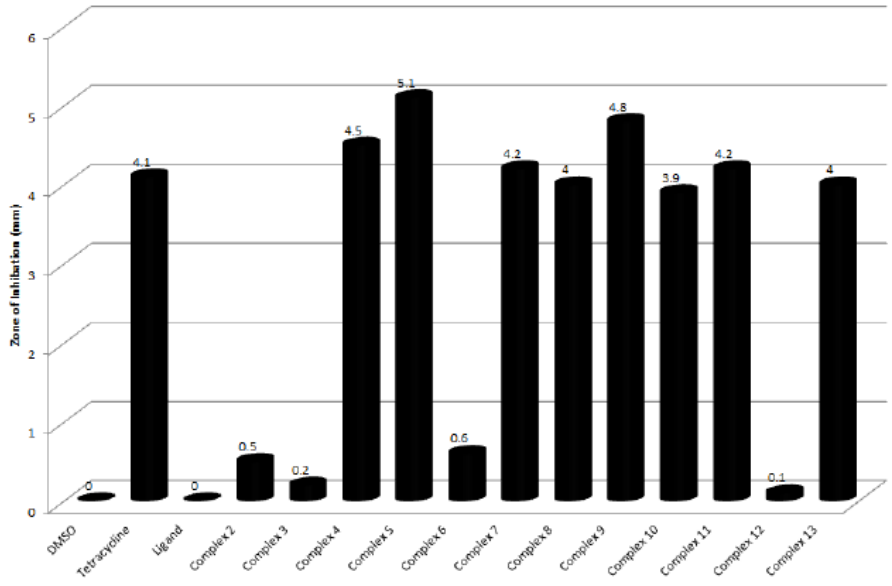

Figure 2. Antibacterial activity of the ligand and its metal complexes against gram-negative bacterium (E. coli).

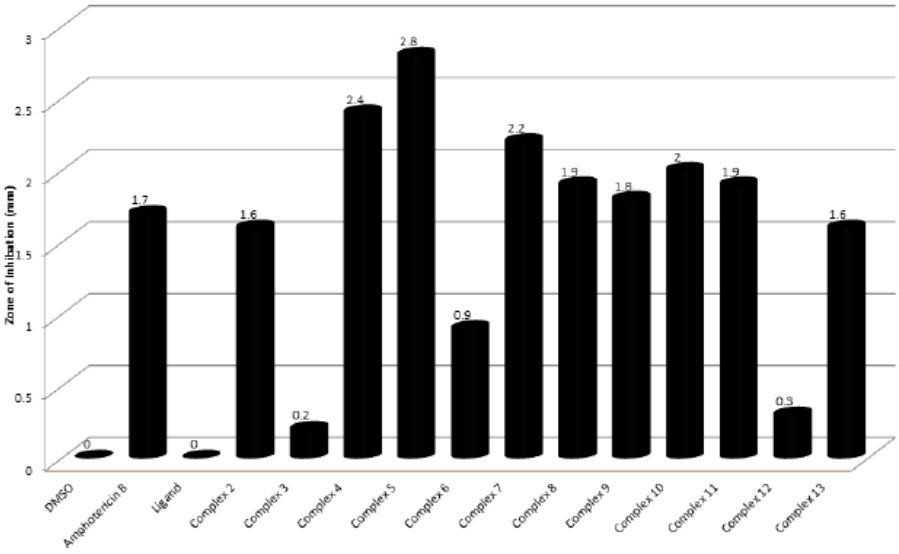

Figure 3. Antifungal activity of the ligand and its metal complexes against Fungus (Aspergillus niger).

The Cu and Ni complexes exhibited the maximum antibacterial and antifungal activities, while Co and Fe complexes showed moderate antibacterial and antifungal activities in this study. The results indicate that the complexes show more activity and the ligands do not have any activity against some organisms under identical experimental conditions. This would suggest that the chelation could facilitate the ability of a complex to cross a cell membrane and can be explained by Tweedy's chelation theory. [59] Chelation considerably reduces the polarity of the metal ion mainly because of partial sharing of its positive charge with the donor groups and possible electron delocalization over the whole chelate ring. Such chelation could also enhance the lipophilic character of the central metal atom, which subsequently favours its permeation through the lipid layer of the cell membrane [60].

CONCLUSION

The ligand H_2L and its corresponding Fe(III), Co(II), Cu(II) and Ni(II) complexes have been synthesized and spectrally characterized. The ligand acted either as bibasic tetradentate, neutral tetradentate. All prepared complexes showed either octahedral or square planar geometries. Complexes 6-10 and 12-13 showed magnetic moments lower than the spin-only value indicating spin-exchange interactions between metal ions. This was more confirmed in case of copper complexes 7-10, which showed G value < 4 suggesting considerable exchange interaction between copper centers in this solid complexes. The values of $g_{//}/A_{//}$ for complexes 5, 7 and 9 lie in the range 126-130 indicating a square planar geometry while the value for complexes 4, 8 and 10 lie in the range 195-214 indicating a octahedral geometry around copper ion. The antibacterial and antifungal activities of the compounds showed that, some of metal complexes exhibited a greater inhibitory effect than the ligand, corresponding aqueous ions, and standard drugs as tetracycline (bacteria) and amphotericin B (fungi).

REFERENCES

[1] Knof U.; von Zelewsky A., "Predetermined Chirality at Metal Centers" *Angew. Chem. Int. Ed*., 38(1999) 302-322.

[2] Knight P.D.; Scott P., "Predetermination of chirality at octahedral centres with tetradentate ligands: prospects for enantioselective catalysis" *Coord. Chem. Rev.*, 242 (2003) 125-143.

[3] You Z-L; Zhu H-L; Liu W-S," Solvolthermal Syntheses and Crystal Structures of Three Linear Trinuclear Schiff Base Complexes of Zinc(II) and Cadmium(II) "Z. *Anorg. Allg. Chem*. 630(2004) 1617- 1622.

[4] Golcu, A.; Tumer, M.; Demirelli, H.; Wheatley, R.A., "Cd(II) and Cu(II) complexes of polydentate Schiff base ligands: synthesis, characterization, properties and biological activity" *Inorganica Chimica Acta*, 358(6), (2005). 1785-1797.

[5] Ziessel R., "Schiff-based bipyridine ligands. Unusual coordination features and mesomorphic behaviour" *Coord. Chem. Rev*., 216 (2001) 195-223.

[6] Parashar R.K.; Sharma R.C.; Kumar A.; Mohan G., "Stability studies in relation to IR data of some schiff base complexes of transition metals and their biological and pharmacological studies" *Inorg. Chim. Acta*, 151(1988) 201-208.
[7] J.R. Lancaster (Ed.), The Bioinorganic *Chemistry of Nickel*, VCH, New York, 1988.
[8] Chandra S.; Sangeetika X., "EPR, magnetic and spectral studies of copper(II) and nickel(II) complexes of schiff base macrocyclic ligand derived from thiosemicarbazide and glyoxal" *Spectrochim. Acta A*, 60 (2004)147-153.
[9] Opstal T.; Verpoort F, "Synthesis of Highly Active Ruthenium Indenylidene Complexes for Atom-Transfer Radical Polymerization and Ring-Opening-Metathesis Polymerization" *Angew. Chem. Int. Ed*., 42 (2003) 2876-2879.
[10] De Clercq B.; Lefebvre F.; Verpoort F., "Immobilization of multifunctional Schiff base containing ruthenium complexes on MCM-41" *Appl. Catal. A* 247 (2003) 345-364.
[11] Lambert S.L.; Spiro C.L.; Gagne R.R.; Hendriekson D.N. "Binuclear complexes of macrocyclic ligands. Variation of magnetic exchange interaction in a series of heterobinuclear CuII-MII complexes" *Inorg. Chem*., 21 (1982) 68-72.
[12] Hodnett E.M.; Dunn W.J., "Improved synthesis of the antibiotic, hexahydrospinamycin" *J. Med. Chem.*, 15 (1972) 339-340.
[13] J.G. Collee, J.P. Duguid, A.G. Farser, B.D. Marmion (editors) "Practical Medical Microbiology" New York, Churchill Livingstone (1989).
[14] F.J. Welcher, *The Analytical Use of EDTA*, Van Norstrand, USA, 1958.
[15] A.I. Vogel, A Text Book of Quantitative Inorganic Analysis, fourth ed., Longman, London, 1978.
[16] Z. Holzbecher, L. Divis, M. Kral, L. Sucha, F. Vlacil, *Handbook of Organic Reagents in Inorganic Analysis*, John Wiley, New York, 1976.
[17] Kannan S.; Ramesh R., "Synthesis, characterization, catalytic oxidation and biological activity of ruthenium(III) Schiff base complexes derived from 3-acetyl-6-methyl-2H-pyran-2,4(3H)-dione" *Polyhedron*, 25 (2006) 3095-3103.
[18] Youssef N.S.; El-Zahany E.; Barsoom B.N.; El-Seidy A.M.A., "Synthesis and characterization of copper(II), cobalt(II), nickel(II), and iron(III) complexes with two diamine Schiff bases and catalytic reactivity of a chiral diamine cobalt(II) complex" *Transition Met. Chem.*, 34 (2009) 905- 914.
[19] K. Nakamoto "Infrared Spectra of Inorganic and Coordination Compounds" 2nd Edit., Wiley - Interscience. New York, 1970.
[20] Abd El-Wahab Z.H.; Mashaly M.M.; Salman A.A.; El-Shetary B.A.; Faheim A.A., "Co(II), Ce(III) and UO2(VI) bis-salicylatothiosemicarbazide complexes: Binary and ternary complexes, thermal studies and antimicrobial activity" Spectrochim. *Acta Part A*, 60 (2004) 2861-2873.
[21] Karvembu R.; Jayabalakrishnan C.; Dharmaraj N.; Renukadevi S.V.; Natarajan K. "Binuclear ruthenium(III) complexes: synthesis, characterisation, catalytic activity in aryl–aryl couplings and biological activity" *Trans. Met. Chem.*, 27 (2002) 631-638.
[22] Youssef N.S.; El-Zahany E.; El-Seidy A.M.A.; Caselli A.; Cenini S., "Synthesis and characterization of some transition metal complexes with a novel Schiff base ligand and their use as catalysts for olefin cyclopropanation" *J. Mol. Catal. A: Chem*. 308(1, 2) (2009) 159-168.
[23] Keskioglu E.; Gunduzalp A.B.; Cete S.; Hamurcu F.; Erk B., "Cr(III), Fe(III) and Co(III) complexes of tetradentate (ONNO) Schiff base ligands: Synthesis,

characterization, properties and biological activity" *Spectrochim Acta A*, 70 (2008) 634-640.

[24] Ramesh R, Maheswaran S "Synthesis, spectra, dioxygen affinity and antifungal activity of Ru(III) Schiff base complexes" (2003) *J. Inorg. Biochem*. 96:457-462.

[25] Teotia M.; Gurthu J.N.; Rama V.B., "Dimeric 5-and 6-coordinate complexes of tri and tetradentate ligands" *J. Inorg. Nucl. Chem*., 42 (1980) 821-831.

[26] EI-Dissouky A.; Fahmy A.; Amer A., "Complexing ability of some γ-lactone derivatives. Thermal, magnetic and spectral studies on cobalt(II), nickel(II) and copper(II) complexes and their base adducts" *Inorg. Chim. Acta*, 133(1987) 311-316.

[27] K. Nakamoto, "Infrared Spectra of Inorganic and coordination compounds", John Wiley and Sons, New York, P 173 (1965).

[28] Boghaei D.M.; Gharagozlou M., "Spectral characterization of novel ternary zinc(II) complexes containing 1,10-phenanthroline and Schiff bases derived from amino acids and salicylaldehyde-5-sulfonates" *Spectrochim. Acta A* 67(2007) 944-949.

[29] Shauib N.M.; Elassar A-ZA.; El-Dissouky A., "Synthesis and spectroscopic characterization of copper(II) complexes with the polydentate chelating ligand 4,4′-[1,4-phenylenedi(nitrilo)dipente-2-one" *Spectrochim. Acta Part A*, 63 (2006) 714-722.

[30] K. Nakamota, "Infrared and Raman Spectra of Inorganic and coordination compounds", 4th Edn, John Wiley and Sons, New York, 1986.

[31] El-Shazly R.M.; Al-Hazmi G.A.A.; Ghazy S.E.; El-Shahawi M.S.; El-Asmy A.A., "Spectroscopic, thermal and electrochemical studies on some nickel(II) thiosemicarbazone complexes" *Spectrochim. Acta A* 61 (2005) 243-252.

[32] Youssef N.S.; El-Zahany E.; El-Seidy A.M.A.; Caselli A.; Fantauzzi S.; Cenini S., "Synthesis and characterisation of new Schiff base metal complexes and their use as catalysts for olefin cyclopropanation" *Inorg. Chim. Acta*, 362 (2009) 2006-2014.

[33] Ferrari M.B.; Fara G.G.; Lafranchi M.; Pelizzi C.; Tarasconi M., "Synthesis, spectroscopic and structural characterization of chlorobis(methyl pyruvate thiosemicarbazone)copper(I) and chlorobis(triphenylphosphine) (methyl pyruvate thiosemicarbazone)copper(I) toluene solvate (2/1)" *Inorg. Chem. Acta*, 181 (1991) 253-262.

[34] Geaey W.J.; "The use of conductivity measurements in organic solvents for the characterisation of coordination compounds" *Coord. Chem. Rev*., 7 (1971) 81-122.

[35] Khalil M.M.H.; Aboaly M.M.; Ramadan R.M., "Spectroscopic and electrochemical studies of ruthenium and osmium complexes of salicylideneimine-2-thiophenol Schiff base" *Spectrochim. Acta Part A*, 61 (2005) 157-161.

[36] Zhang H-Y.; Wu K-Z.; Zhang J-J.; Xu S-L.; Ren N.; Bai J-H.; Tian L, "Synthesis, crystal structure and thermal decomposition kinetics of the complex [Sm(BA)3bipy]2" *Synthetic Metals*, 158 (2008) 157-164.

[37] Wu G.; Wang X.; Li J.; Zhao N.; Wei W.; Sun Y, "A new route to synthesis of sulphonato-salen-chromium(III) hydrotalcites: Highly selective catalysts for oxidation of benzyl alcohol to benzaldehyde" *Catal. Today*, 131 (2008) 402-407.

[38] Mostafa S.; Ikeda S.; Ohtani B, "Transition metal Schiff-base complexes chemically anchored on Y-zeolite: their preparation and catalytic epoxidation of 1-octene in the suspension and phase boundary systems" *J. Mol. Catal. A: Chem.,* 225 (2005) 181-188.

[39] Mohamed G.G.; El-Wahab Z.H.A., "Mixed ligand complexes of bis(phenylimine) Schiff base ligands incorporating pyridinium moiety: Synthesis, characterization and antibacterial activity" *Spectrochim. Acta Part A*, 61(6) (2005) 1059-1068.
[40] Tascioglu S, Yalcin B, Nasrullayeva TM, Andac O, Buyukgungor O, Aydin A, Medjidov AA (2006) *Polyhedron*, 25(6):1279.
[41] B. P. Lever, "Inorganic Electronic Spectroscopy", Elsevier, Amsterdam, 341, (1968).
[42] Shakir M.; Azim Y.; Chishti H-T-N.; Parveen S., "Synthesis, characterization of complexes of Co(II), Ni(II), Cu(II) and Zn(II) with 12-membered Schiff base tetraazamacrocyclic ligand and the study of their antimicrobial and reducing power" (2006) *Spectrochim. Acta Part A*, 65:490-496.
[43] Kumar K.G.; John K.S., "Complexation and ion removal studies of a polystyrene anchored Schiff base" *Reactive and Functional Polymers 66*(12) (2006) 1427-1433.
[44] F.A. Cotton, G. Wilkinson, Advanced Inorganic Chemistry, John Wiley and Sons, New York, 1998.
[45] Mostafa SI, Ikeda S, Ohtani B "Transition metal Schiff-base complexes chemically anchored on Y-zeolite: their preparation and catalytic epoxidation of 1-octene in the suspension and phase boundary systems" *J. Mol. Catal. A*, 225 (2005)181-188.
[46] Mohamed G.G.; Omar M.M.; Hindy A.M.M., "Synthesis, characterization and biological activity of some transition metals with Schiff base derived from 2-thiophene carboxaldehyde and aminobenzoic acid" *Spectrochim. Acta Part A*, 62 (2005) 1140-1150.
[47] Mohamed G.G.; El-Wahab Z.H.A., "Mixed ligand complexes of bis(phenylimine) Schiff base ligands incorporating pyridinium moiety: Synthesis, characterization and antibacterial activity" *Spectrochim. Acta Part A*, 61 (2005) 1059-1068.
[48] Amirnasr M, Schenk KJ, Meghdadi S, Morshedi M "Synthesis, characterization and X-ray crystal structures of [Ni(Me-sal)2dpt] and [Ni(Me-sal)dpt]Cl" *Polyhedron* 25 (2006) 671-677.
[49] Bouwman E.; Henderson R.K.; Reedijk J.; Veldman N.; Spek A.L., "Synthesis of the ligand N,N′-bis(2-tert-butylthiobenzenylidene)-diethylenetriamine; its reactivity with nickel(II) salts" *Inorg. Chim. Acta* 287 (1999) 105-108.
[50] B. P. Lever "Inorganic Electronic Spectroscopy" 2nd edn, Elsevier, Amsterdam, 1984.
[51] Kumar K.G.; John K.S., "Complexation and ion removal studies of a polystyrene anchored Schiff base" *React. Funct. Polym.* 66 (2006) 1427-1433.
[52] Nair M.S.; Joseyphus R.S., "Transition metal Schiff-base complexes chemically anchored on Y-zeolite: their preparation and catalytic epoxidation of 1-octene in the suspension and phase boundary systems" *Spectrochim Acta* A 70 (2008) 749-188.
[53] Youssef N.S.; El-Zahany E.; El-Seidy A.M.A., "Synthesis and characterization of new schiff base metal complexes and their use as catalysts for olefin cyclopropanation" Phosphorus, Sulfur Silicon *Relat. Elem*. 185 (2010) 785-798.
[54] Chandra S.; Kumar U., "Spectral and magnetic studies on manganese(II), cobalt(II) and nickel(II) complexes with Schiff bases" *Spectrochim. Acta* A, 61 (2005) 219.
[55] Patel R.N.; Singh N.; Gundla V.L.N., "Synthesis, structure and properties of ternary copper(II) complexes of ONO donor Schiff base, imidazole, 2,2′-bipyridine and 1,10-phenanthroline" *Polyhedron*, 25 (2006) 3312-3318.
[56] Kivelson .D; Neiman R., "ESR Studies on the Bonding in Copper Complexes" *J. Chem. Phys.* 35 (1961) 149-156.

[57] Cozar, O.; David, L.; Chiş, V.; Cosma, C.; Znamirovschi, V.; Damian, G.; Bratu I.; Bora Gh., "ESR study of some solvent effects of the Cu(II)-aspirinate complex" *Appl. Magn. Reson.*, 8 (1995) 235-242.

[58] A.W. Addison, in: K.D. Karlin, J. Zubieta (Eds.), Copper Coordination Chemistry Biochemical and Inorganic Perspectives, Adenine Press, New York, 1983.

[59] Fahmi N.; Gupta I.J.; Singh R.V., "Sulfur bonded palladium(ii) and platinum(ii) complexes of biologically potent thioamides" *Phosphours Sulfur and Silicon*., 132 (1998) 1-8.

[60] Tumer M.; Ekinci D.; Tumer F.; Bulut A., "Synthesis, characterization and properties of some divalent metal(II) complexes: Their electrochemical, catalytic, thermal and antimicrobial activity studies" *Spectrochimica Acta* A 67(3-4) (2007) 916.

Smart Nanocomposites
Volume 3, Number 1
ISSN: 1949-4823

SYNTHESIS OF 2-AMINOTHIAZOLE DYE AND ITS METAL COMPLEXES AS AGENTS FOR ORGANIC/INORGANIC HETEROJUNCTION

Fathy A. El-Saied[1*], Ehab Abdel-Latif[1], Ahmed M. Nawar[2], Ahmed S. Radwan[1] and Atef A. Hamed[1]

[1]Chemistry Department, College of Science, Qassim University, Saudi Arabia, KSA
[2]Thin Film Laboratory, Physics Department, Faculty of Science,
Suez Canal University, Ismailia, Egypt

ABSTRACT

2-Acetylamino-5-phenylazo-thiazole (HL) was synthesized by acetylation of 2-amino-5-phenylazo-thiazole with acetic anhydride. Metal complexes of Cu(II), Co(II), Ni(II) and Fe(III) with the ligand have been prepared and characterized using variety of analytical, spectral, magnetic and thermal techniques. The obtained data show that the reaction of ligand with metal ions led to the formation of 1:1 or 1:2 (metal: ligand) metal complexes were formed. The results also show that in Cu(II) complex, the ligand behaves as a monobasic tridentate ligand coordinating via the azo nitrogen atom, sulfur atom and the enolic oxygen atom (NSO mode).Whereas, in case of complexes of Co(II), Ni(II) and Fe(III), the ligand behaves as a neutral bidentate, coordinating through the azo nitrogen and sulfur atoms (NS mode). Hybrid heterojunction cells based on the spin-coated dye and its metal complexes as the organic semiconductor on p-Si wafers as the inorganic semiconductor have been fabricated and investigated at room temperature 293 °K. The AFM atomic force microscopy measurements showed that the spin-coated dye and its metal complexes contain a wide range of nano-sized particles. The fabricated devices showed rectification behavior like diode. The diode parameters have been studied using current–voltage (I–V) characteristics in dark and under illumination at room temperature 293 °K. The photovoltaic parameters of all prepared Au/ spin-coated ligand or complex /p-Si/Al devices were investigated under illumination with a light intensity of 6 mW/cm^2. One of the synthesized materials showed a promising behavior for the photovoltaic applications with efficiency 3.3%.

Keywords: Thiazole; Diazonium chloride; Dyes; metal complexes; Organic/inorganic heterojunction; Photovoltaic

[*] Corresponding Author : Fathy A. El-Saied, E-mail address: fathi_elsaied@yahoo.com

1. INTRODUCTION

Metal–semiconductor junctions have been commonly used in microelectronic devices and in creating important circuit elements including ohmic contacts, Schottky diodes, and metal semiconductor field-effect transistors. Upon the introduction of organic modification to semiconductor materials, research has been very active with an ultimate goal to molecularly manipulate the formation, operation, and tenability of metal–molecule–semiconductor devices [1]. Control over the electronic properties of semiconductors and a metal is a central issue for their use in electronic devices [2]. The use of molecules to modify and tailor material properties is attractive in electronic devices because of the molecules' functional variety and flexibility. The use of molecules to control electron transport is an interesting possibility, not least because of the anticipated role of molecules in future electronic devices [3]. It has been demonstrated that molecules can control the electrical characteristics of conventional metal–semiconductor junctions [2,4], apparently without the need for electrons to be transferred onto and through the molecules. Diodes have been modified by adsorbing small molecules onto single crystals of n-type GaAs semiconductor [4]. Organic materials have been also intensively investigated due to their wide range of applications in electronics technology [5-9] disordered Semiconductors. Organic semiconductors are being explored for a number of exciting applications, such as organic light-emitting diodes (OLEDs), organic thin film transistors (OTFTs), and organic photovoltaics (OPVs). A salient feature distinguishing organic (including polymeric) semiconductors from their inorganic counterparts is the strong tendency of charge carrier localization in the former. The effects of carrier localization are reflected by the dominant role of polarons due to electronic nuclear coupling. The inherent tendency for carrier localization is enhanced by the presence of energetic disorder, which is the result of structural inhomogeneities and chemical impurities, leading to charge carrier trapping in some cases. Thus, we can view organic semiconductors as members of the disordered semiconductor family [10]. Interfacial layers are used between the photoactive BHJ layer and the electrodes in order to adjust the energy levels between the electrode and the active layer and to enhance charge derivatives show biological significance, e.g., they are found in the penicillin and vitamin B1 molecules and in coenzyme cocarboxylase [11]. The chemistry extraction [12] and planarise the surface of the underlying electrode [13]. Thiazole and its of 2-thiazolines, including new methodologies for their preparation, and recent applications, such as their growing use in organic synthesis in the biological field and asymmetric catalysis as ligands has been recently reviewed [14]. 2-Aminothiazoles are known mainly as biologically active compounds with a broad range of activity and as intermediates in the synthesis of antibiotics and dyes [15]. Several papers have been published on the use of these compounds as antimicrobial [16], antifungal [17], anti-inflammatory activity [18], anesthetic [19] and antiviral drugs [20]. 2-Aminothiazoles and its derivatives are also used in the syntheses of various types of dyes [21-24]. Furthermore, high-density optical data storage has been a subject of extensive research in the past decade, In general, cyanine dyes, phthalocyanine dyes, and metal-azo complex dyes are used in the recording layer of DVD-R (Digital Versatile Disc –Recordable) discs. It has been reported that the new technology, which employs 405 nm blue-violet diode lasers, requires a new optical recording medium matching 405 nm wavelength laser. In comparison with the dyes themselves, metal azo dyes are more light stable, allowing easier control to the wavelength by selection of the appropriate azo compounds and the ease

with which the absorption band may be tuned by varying the substituents, one of the many applications of azo compounds is the optical data storage. In other words, the thermal substituent groups, and have good thermal stability [25-29] Because of the good thermal properties and suitable absorption band of azo compounds are essential features in relation to their application at high-density optical recording materials. In this work, 2-acetylamino-5-phenylazo-thiazole (HL) ligand and its Cu(II), Co(II), Ni(II) and Fe(III) complexes were synthesized and characterized by using analytical , spectral, magnetic and thermal measurements. a hybrid solar cell was designed as shown schematically in Figure 1.a The electrical properties of heterojunctions were characterized by measuring the current density–voltage (J–V) curve in the dark and under illumination. The J–V curve in the dark is the easy way to estimate the quality of the junction, grid and contact resistances. Also, the basic parameters including open-circuit voltage (V_{oc}), short-circuit current density (J_{sc}), fill factor (FF) are usually determined through three points on the J–V curve under illumination. Analysis of the J–V curve gives not only the basic parameters, but also the extracted parameters such as reverse saturation current, J_o, series resistance, R_s, shunt resistance, R_{sh}, and ideality factor, n. These parameters can be applied in turn to improve the device quality during fabrication and the solar cell performance [30-33].

2. EXPERIMENTAL

2.1. Instrumentation

All melting points were measured on an electrothermal Gallenkamp melting apparatus. Elemental analyses were carried out at the Microanalytical Unit, Faculty of Science, University of Mansoura, Egypt; the results were in satisfactory agreement with the calculated values. UV–visible spectra were recorded with a Perkin-Elmer Lambda 551 S spectrometer in the solid state dispersed on njull mull. IR spectra (KBr discs) were determined on a Mattson 5000 FTIR spectrometer). The 1H NMR spectra were acquired using a Bruker WP 300 spectrometer at 300 MHz using TMS as an internal standard. Thermogravimetric analyses (TGA) of the solid complexes was recorded using Shimadzu TG-50 Thermogravimetric Analyzer with heating rate 10°C / min under nitrogen atmosphere, in the range 25-1000°C. Magnetic susceptibilities of the complexes were measured at room temperature in the polycrystalline state in a borosilicate tube using Johnson Matthey Magnetic Susceptibility Balance. Magnetic susceptibility was measured and calculated by using the following equation [34].

$$\mu_{eff} = 2.828\ (\chi_n \times T)^{1/2}$$

$$\chi_a = [1.115\ L(R-R_o)]/W\times 109\ ,\ \chi_m = \chi_a \times MW\ ,\ \chi_n = \chi_m - D$$

where: χ_a = mass susceptibility, L = sample length in cm, R = tube + sample reading ,R_o = empty tub reading ,W = mass of the sample ,χ_m = molar susceptibility, MW = Molecular weight , χ_n = corrected molar susceptibility D = diamagnetic correction, μ_{eff} = effective magnetic moment, T = room temperature in Kelvin (˚k)

The theoretical effective magnetic moment value calculated using the equation

$\mu_{eff} = [n(n+2)]^{1/2}$,

where: μ_{eff} = theoretical effective magnetic moment; n = the number of the unpaired electrons. Diamagnetic corrections were made using Pascal's constants [35]. Molar conductance measured by using Hanna HI8733 conductivity meter 1999.9 μs temperature coefficient = 1.

2.2. Synthesis of the Organic Dye (HL)

2.2.1. Synthesis of 2-Amino-5-Phenylazo-Thiazole (2)

A solution of phenyl diazonium chloride was prepared by adding cold sodium nitrite solution (0.7 g in 10 ml H_2O) to a cold suspension of 0.93 ml aniline in 3 ml concentrated HCl with stirring.

The freshly prepared solution was added with continuous stirring to a cold solution (0-5°C) of 2-aminothiazole (0.01 mol) in 30 ml ethanol and 4.0 g sodium acetate. The reaction mixture was stirred at 0-5°C for 2 hours, diluted with water, and then filtered. 2-Amino-5-phenylazothiazole (2) thus obtained, was dried and recrystallized from ethanol. Yield 86%; mp 270-271°C; IR (KBr): $\bar{\nu}$ = 3421, 3270 (NH2), 1639 (CO) cm-1; 1H NMR (DMSO-d_6): δ = 6.90 (s, C_4-H, thiazole), 7.05-7.40 (m, Ar-H), 8.35 (d, NH2) ppm.

2.2.2. Synthesis of 2-Acetylamino-5-Phenylazo-Thiazole (3) (HL)

A mixture of 2-amino-5-phenylzothiazole (2, 0.01 mol) and 10 ml acetic anhydride was heated in an oil bath at 60-65°C for 1 hour.

The reaction mixture was allowed to cool at room temperature and then recrystallized from ethanol to afford the corresponding 2-acetylamino-thiazole derivative (HL).Yield 78%; mp 233-235°C; IR (KBr): $\bar{\nu}$ = 3280 (NH), 1697 (CO), 1562 (C=N) cm-1; 1H NMR (DMSO-d6): δ = 1.80 (s, CH3), 6.85 (s, C4-H, thiazole), 7.10-7.45 (m, Ar-H), 11.40 (s, NH) ppm. Steps of preparation of ligand are shown in Scheme (1).

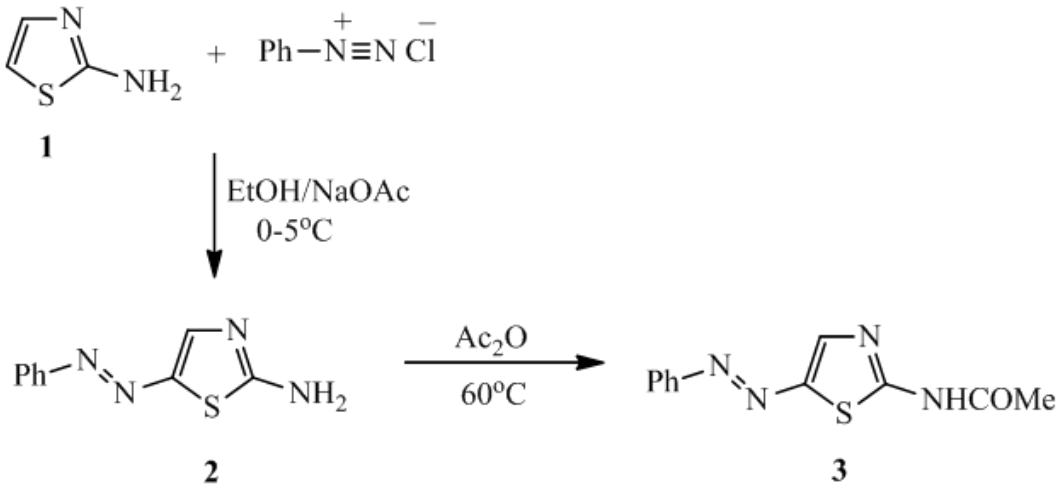

Scheme 1.

2.3. Preparation of Metal Complexes

Cu(II) , Co(.II), Ni(II) and Fe(III) complexes of HL were prepared by adding 0.1 mol (0.246 g) of ligand dissolved in 50 ml of ethanol to 0.1 mol of the appropriate metal salt dissolved in a least volume of ethanol .The reaction mixture is heated under reflux for about 1-2 hrs. The precipitated product was filtered off, washed several times with ethanol and dried under vacuum in presence of anhydrous $CaCl_2$.

2.4. Heterojunctions Preparation

To obtain an Au/org/inorg/Al cell, the sample has been prepared by using a polished p-type Si wafer with (100) orientation and hole concentration of $1.6 \times 10^{23} m^{-3}$ with thickness of 400 μm as an inorganic semiconductor. In order to remove the native oxide on p-Si surface, the substrate was etched by CP_4 solution (HF: HNO_3: CH_3COOH in ratio 1:6:1) for 10 s, then rinsed with deionized water and isopropyl alcohol and dried in oven. After the drying method all the p-Si pieces were inserted in Edward E306A, England coating unit in order to fabricate the Al-back contact. This was made by depositing a relatively thick film of Al to the bottom of fifteen p-Si substrates; Evaporation of Al is carried out heating the aluminum wire by a tungsten coil under vacuum of 2×10^{-5} Pa. The evaporation rates as well as the film thickness of the evaporated films were controlled by using a quartz crystal monitor FTM6, the deposition rate was controlled at 0.5 nm/s. After the preparation of the Al-back contact, the samples were inserted in a quartz tube to be annealed in oven under 723 K for 3 min under vacuum of 3×10^{-4} Pa.

The prepared powders were dried at 333 K under roughing vacuum for 5 h then dissolved in DMF with concentration of 30 mg/ml. Figure 1(a) shows the variation of colour occupancy of the prepared dyes in the used transparent bottles. The nano-dyes thin films were deposited by spin-coating technique; was spin-coated on the top of p-Si/Al with a speed of 1500 rpm for 45 s. After finishing the previous step, all samples (HL/p-Si/Al, complex(4)/p-Si/Al, complex(3)/p-Si/Al, complex(5)/p-Si/Al and complex(2)/p-Si/Al) were annealed under roughing vacuum at 353 K; in order to improve the dyeability of the top of p-Si/Al and adhesivity of the dye-film to the top of p-Si/Al. Note, each one of the prepared solution of the prepared dyes was used to prepare a thin film on a three samples of the org/inorg/Al, in order to accurately, investigate the modification of the synthesized dyes for the barrier height between the Au/org and the p-Si/Al of the fabricated heterojunctions. Finally, the Au-wire was thermally evaporated by a tungsten coil under vacuum of 2×10^{-5} Pa to fabricate Au films with an area of 0.06 cm^2 on the spin coated dye-films. The device had the same structure as the previous published works of the fourth author (see Ref. [6]). Figure 1(b) shows a simple diagram for the structure of Au/org-dye or complex:Si-p/Al Org/Inorg heterojunction.

Surface topography was studied by contact mode atomic force microscopy AFM in (Engineering and Surface Metrology Department, National Institute for Standards, Egypt). The collected 3D topographical data was analyzed using data analysis software (IP; Image Processing and Data Analysis, V.2.1.15, Thermo Microscopes, CA, USA) and SPIP software (Image Metrology). Nano-roughness data was calculated over the whole image (area), with cited numbers resulting from at least three images of 0.5×0.5 μm^2. Plane correction was applied to each image before the roughness calculations [36].

HL = L_2, E_2= complex 4, E_7= complex 2, E_{23}= complex 3, E_{28}= complex 5

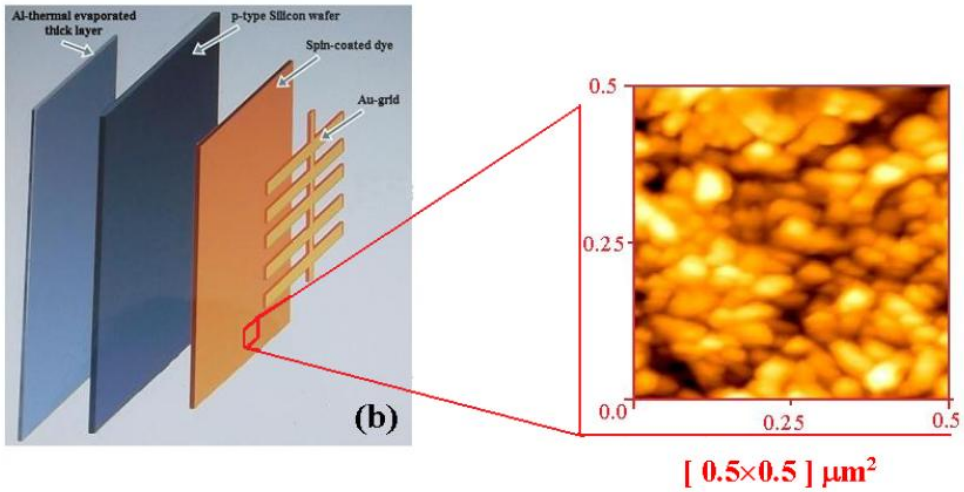

Figure 1. Shows the prepared solutions of the synthesized organic dyes and Org/Inorg-heterojunction structure (a) Suspensions of nearly monodisperse organic dyes, and (b) Schematic structure of the required parts for the Org/Inorg-heterojunctions solar cell devices with gold-mesh. The inset shows the Atomic force microscopy (AFM) image of the E_7-dye, formed with the spin-coating method on p-Si substrate with 0.5×0.5 μm^2 scan size, as a representative sample.

The obtained cell was annealed in air at 353 K for 1 h to complete the junction formation. Annealing of heterojunction has been the usual step in obtaining the best efficiency cells. This annealing might remove any channels, which could be raised during the fabrication [6,37]. In addition, thermal annealing condition was found very important for improving short circuit current, fill factor, and therefore the efficiency of the device [38]. The dark current–voltage (I–V) characteristics of the fabricated cell were measured simultaneously using a high impedance electrometer (Keithley 6517 B). The dark I–V characteristics were obtained in a complete dark chamber at room temperature or inside a dark furnace in case of measurements at higher temperatures.

The illuminated (I–V) characteristics are carried out by using (Keithley 6517 B) under intensity of light =6 mW/cm^2 provided by a tungsten lamp. The intensity of the incident light was measured by using digital lux-meter (BCHA, model 93408).

3. RESULTS AND DISCUSSION

3.1. Structure Investigation and Spectral Studies of Prepared ligand (HL)

3.1.1. Elemental Analysis of Ligand (HL)

The prepared organic ligand was purified by recrystallization from ethanol. The obtained results of elemental analysis, which are listed in Table 1, confirm the purity of the prepared organic ligand.

3.1.2. IR Spectrum of ligand (HL)

The IR spectrum of the ligand was recorded in the solid state as potassium bromide discs, within the range 4000-200 cm^{-1}. The assignment of the most diagnostic IR absorption bands were listed in Table 1.

The infrared spectrum of the ligand shows bands at 3159 and 3280 cm^{-1} that assigned to υ(NH) . The spectrum of the ligand also shows strong bands at 1697, 1562, 1435 and 790 cm^{-1} corresponding to υ(C=O) , υ(C=N)of the ring , υ(N=N) and υ(C-S) of the ring, respectively.

3.2. Elucidation of Structure of Metal Complexes

3.2.1. Elemental Analysis and Molar Conductivity

The reactions of the ligand HL with different metal ions ; $Cu(NO_3)_2$, $CoCl_2$, $NiCl_2$, and $FeCl_3$, in molar ratios 1:1 gave complexes shown in Table 1. As shown in Table 1 and Scheme 2, the reaction of ligand with $Cu(NO_3)_2$and $CoCl_2$ led to the formation of 1:1 molar ratio, whereas, with $NiCl_2$ and $FeCl_3$, 1:2 metal complexes were formed . The obtained metal complexes are air stable, non-hygroscopic and partially soluble in water and most organic solvents except dimethylformamide (DMF) and dimethylsulphoxide (DMSO), where they are freely soluble.

The values of molar conductivities in DMF (10^{-3} M) solutions which are listed in Table 1, indicate that all metal complexes except, complex (5) are non-electrolytes[39], indicating that all anions in metal complexes are directly attached to the metal ion. The value of molar conductivity of complex (5) is 87 $ohm^{-1}cm^2mol^{-1}$ indicating that the solution of the complex is 1:1 electrolyte, and one chloride ion presents in the outer sphere [40].

3.2.2. Infrared Spectra

The bonding mode of the ligand in the metal complexes has been deduced by comparing the infrared spectra of metal complexes with that of the free ligand. The most diagnostic infrared spectral bands for ligand and its metal complexes and their assignments are listed in Table 2.

The data listed in Table 2 showed that, the infrared spectra of all metal complexes of ligand HL , reveal that the bands ascribed to υ(N=N) at a higher frequency and υ(C-S) band at a lower frequency compared to that of the free ligand, indicating that coordination via the azo group and sulfur atoms occurred.

Table 1. Elemental analysis, color, molar conductivity and molar ratio for ligand and its metal complexes

No	Compounds	color	Λ_M	Salt	Molar ratio	Elemental analysis			
						C %	H %	N %	M%
1	HL	orange	-	-	-	54.0 (53.7)	3.8 (4.1)	22.6 (22.8)	-
2	[CuHL (NO_3)]	brown	20.3	$Cu(NO_3)_2$	1:1	36.1 (35.6)	3.1 (2.7)	18.1 (18.9)	17.5(17.1)
3	[$CoHLCl_2(H_2O)_2$]	red	19.5	$CoCl_2$	1: 1	32.7 (32.1)	2.9 (3.4)	14.3 (13.6)	14.5(14.3)
4	[$Ni(HL)_2Cl_2$]	green	15.3	$NiCl_2$	1:1	41.9 (42.5)	3.2 (3.2)	17.7 (18.0)	10.0(9.4)
5	[$Fe(HL)_2Cl_2$]Cl	brown	87	$FeCl_3$	1:1	41.0 (40.3)	3.3 (3.1)	17.3 (17.1)	9.1(8.6)

Λ_M = molar conductivity, $ohm^{-1}cm^2mol^{-1}$.

Table 2. Infrared spectral bands for ligand and its metal complexes

No	Compound	υ (N - H)	υ (C= O)	υ (C=N)	υ (N=N)	υ (C- S)	υ (M-S)/ υ (M-O)	υ (M-N) / υ (M-S)
(1)	HL	3159, 3280	1697	1562	1435	790	-	
(2)	[$CuL(NO_3)$]	-	-	1651, 1580	1470	771	410, 509	455, 410
(3)	[$Co(HL)Cl_2(H_2O)_2$]	3155, 3420[a]	1697	1562	1455	767	410	440, 410
(4)	[$Ni(HL)_2Cl_2$]	3271, 3200	1708	1570	1473	767	420	445, 420
(5)	[$Fe(HL)_2Cl_2$]Cl	3155	1697	1562	1450	768	405	467, 405

[a] = υ (OH) of coordinated water.

Table 3. Magnetic moment values and electronic spectral bands of metal complexe in the solid state

No	Complex	μ_{eff} (B.M) per metal ion	d-d bands (nm)
(2)	$[CuL(NO_3]$	1.78	570 (br)
(3)	$[Co(HL)Cl_2(H_2O)]$	4.98	680(w), 580(w)
(4)	$[Ni(HL)_2Cl_2]$	2.98	830, 664
(5)	$[Fe(HL)_2Cl_2]Cl$	5.71	690, 530

br= broad, w= weak.

The spectrum of complex (2) shows that the two bands corresponding to υ(N-H) and υ(C=O) disappeared and a new band appeared at 1651cm^{-1}, assigned to υ(C=N) upon complexation, indicating that the ligand in this complex reacted in the enol form via the enolic oxygen atom , N=N and sulfur atom .The infrared spectra of complexes (3), (4), and (5) show that the bands characteristic to υ(C=N) of the ring and υ(C=O) appeared approximately at the same positions as that of the free ligand, indicating that they don't participate in coordination.

The above arguments together with the results of elemental analyses indicate that, the ligand HL behaves as a monobasic tridentate , coordinating via the sulfur atom, azo nitrogen atom and enolic oxygen atom (NSO mode) or as a neutral bidentate, coordinating through the sulfur atom and azo nitrogen atom (SN mode). The rest coordinations are satisfied by chloride ions, nitrate and /or water molecules to complete the coordination number. The presence of water molecules within the coordinated sphere in the hydrated complexes (3) is supported by the appearance of infrared spectral bands at 3420 cm^{-1}, 885 cm^{-1}, and 695 cm^{-1}, assigned to OH stretching , H_2O rocking and H_2O wagging, respectively [41]. The spectra of complexes show two new bands at 467 – 440 cm^{-1} and 420 -405 cm^{-1}, assigned to υ(M-N) and υ(M-S), respectively [42]. The spectrum of complex (2) shows additional new band at 509 cm^{-1}, assigned to υ(Cu-O) [42].

3.2.3. Magnetic Moments and Electronic Spectral Data for Metal Complexes

The electronic absorption spectral bands as well as the room temperature magnetic moments (μ_{eff} B.M.) per a metal atom of the metal complexes are listed in Table 4.

The magnetic moment value for the copper(II) complex (3) is 1.78 B.M.. The value of magnetic moment of complex is consistent with the spin only value (1.73 B.M.), correspond to one unpaired electron [43] in a square planar or octahedral geometry [44]. Value also indicates that no exchange interactions occurs between copper ions. The electronic spectrum of copper(II) complex shows a broad band at 570 nm, which suggests a square planar geometry around the copper(II) ion[45].

Octahedral, tetrahedral and square planar cobalt(II) complexes show magnetic moment values between 4.7 – 5.2, 4.2 – 4.8 and 2.2 – 2.9 B.M., respectively [46-48]. The room temperature magnetic moment value for cobalt (II) complex (3) is 4.98 B.M . This value is indicative for an octahedral geometry around the cobalt(II) ion .The considerably high value ruled out any spin- spin interactions between cobalt(II) ions. The electronic spectrum of cobalt(II) complex shows two weak bands at 680 and 590 nm which may be assigned to $^4A_2g \rightarrow {}^4T_{1g}$ (P) (υ_3) and $^4T_{1g} \rightarrow {}^4A_{2g}$ (υ_2), respectively, which is indicative for octahedral cobalt(II) geometry [49].

Table 4. TGA data of some metal complexes

No	Complex	Temperature (˚C)	Weight loss found (calcd.) %	Species removed or formed
(2)	$[CuL(NO_3)]$	30- 164 164-240 240-872 872	- 17.2(16.7) 65.9(66.4) -	Stable -1 NO_3 -1 ligand CuO formed
(3)	$[Co(HL)Cl_2(H_2O)_2]$	30-250 250-305 305-951 951	- 26.8 (26.0) 60.7(59.8) -	stable - 2 H_2O +2 Cl - ligand CoO formed
(4)	$[Ni(HL)_2Cl_2]$	30-300 300 -900 900	- 78.9 (79.8) -	stable - 2 Cl +2 ligand -NiO formed

The nickel(II) complex was found to be paramagnetic which excludes the possibility of a square planar configuration. The room temperature magnetic moment value of nickel(II) complex (4) is 2.98 B.M.

Six-coordinate nickel(II) complexes generally exhibit three d–d bands in the Vis.-NIR region corresponding to the $^3A_{2g}(F)\rightarrow{}^3T_{2g}(F)$ (υ_1), $^3A_{2g}(F)\rightarrow{}^3T_{1g}(F)$ (υ_2) and $^3A_{2g}(F)\rightarrow{}^3T_{1g}(p)$ (υ_3) transitions. However nickel(II) complex (4) displays only two bands at 664 and 830 nm, which are attributable to $^3A_{2g}(F)\rightarrow{}^3T_{1g}(F)$ (υ_2) and $^3A_{2g}(F)\rightarrow{}^3T_{1g}(p)$ (υ_3) transitions, respectively indicating an octahedral nickel(II) complex. The third one does not observe possibly because it is out the range of spectrophotometer (> 900 nm) [50,51]. Iron(III) complex (5) shows bands at 530 and 690 nm assigned to $_6A_{1g}\rightarrow{}_4T_{2g}(G)$ and $^6A_1(G)\rightarrow{}_4T_1(G)$ transitions, characteristic of octahedral iron(III) [50,52]. The iron(III) complex (5) gave magnetic moment value 5.71 BM, compatible with high-spin d^5 iron(III) ions.

3.2.4. Thermal Analysis

The TGA results for some of the solid complexes (**2**), (**3**) and (**4)** are listed in Table 4. The results show good agreement with the formulae suggested from the analytical, spectral and magnetic data. A general decomposition pattern was concluded, whereby the complexes decomposed in stages. The first decomposition stage is the loss of the NO_3^- or Cl^- anions at 164-305 °C. The second decomposition stage is the loss of molecules of ligand at temperature range 240 -951 °C for all complexes.

Finally, metal-oxide formation takes place. Complexes (**2**),(3) and (4) show thermal stability up to 164, 250 and 300 ˚C respectively. The above arguments confirmed the chemical formulas of metal complexes as shown in Scheme 2.

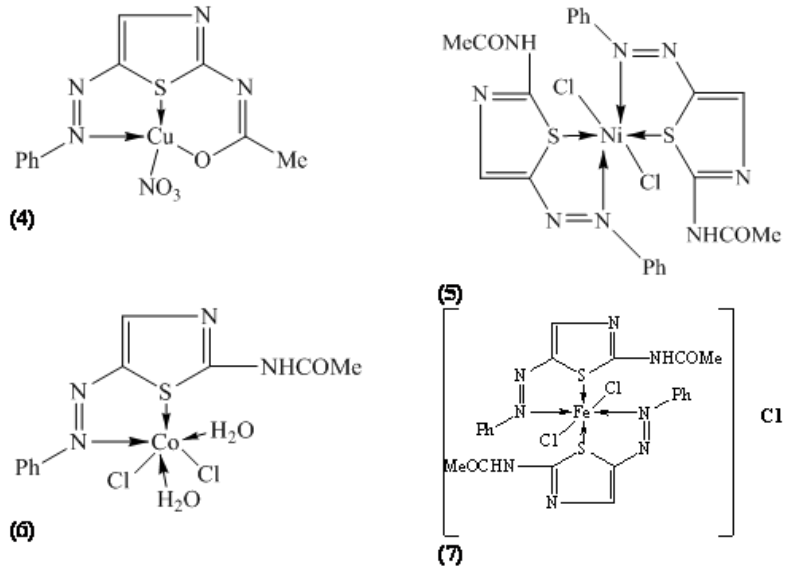

Scheme 2.

3.3. Effects of Annealing Temperature on Topological Properties of the Prepared Compounds

The inset of Figure 1(b) shows a two-dimensional Topographical image for complex (2) on p-Si/Al as a representative sample. This figure depicts the effects of annealing temperature at 253 K on the surface topography of the spin coated complex (2) synthesized complex as a representative sample. Table 1 shows the recorded parameters which are based on two-dimensional standards. The values of R_q and $R_{p\text{-}v}$ are decreased by amounts of 1.45 and 8.7 nm, respectively, (may be due to the aggregate densification effect of the annealing temperature 353 K). Also The valley depth (R_v) and peak profile (R_p) are decreased by amounts of 3.38 and 5.3 nm, respectively. In conclusion, the annealing temperature at 353 K decreases the surface roughness R_q, mean peak-to-valley profile roughness $R_{p\text{-}v}$ and mean half wavelength (S_{hw}) of the as-deposited NiTPP thin films by 23.27 %, 21.9 % and 25.17 % respectively. All analyzed data for the annealed complex (2) spin-coated film on p-Si/Al thin films are limited to the annealing temperature at 353 K in a roughing vacuum. In conclusion, the thermal annealing can modify the surface topographies of the spin-coated films by controlling the aggregate densification and porous properties of the organic dye [37].

3.3. Dark I–V Characteristics of the Prepared Org/Inorg Heterojunctions

Figure 2 shows the typical current–voltage (I–V) characteristic observed for the prepared heterojunctions under the forward and reverse bias measured for all prepared devices and in the voltage range −2 to 2 V. The device exhibits rectification behaviour whereby the current–voltage (I–V) characteristics are limited by the properties of the inorganic semiconductor substrate and the magnitude of the energy barriers at the hetero-interface.

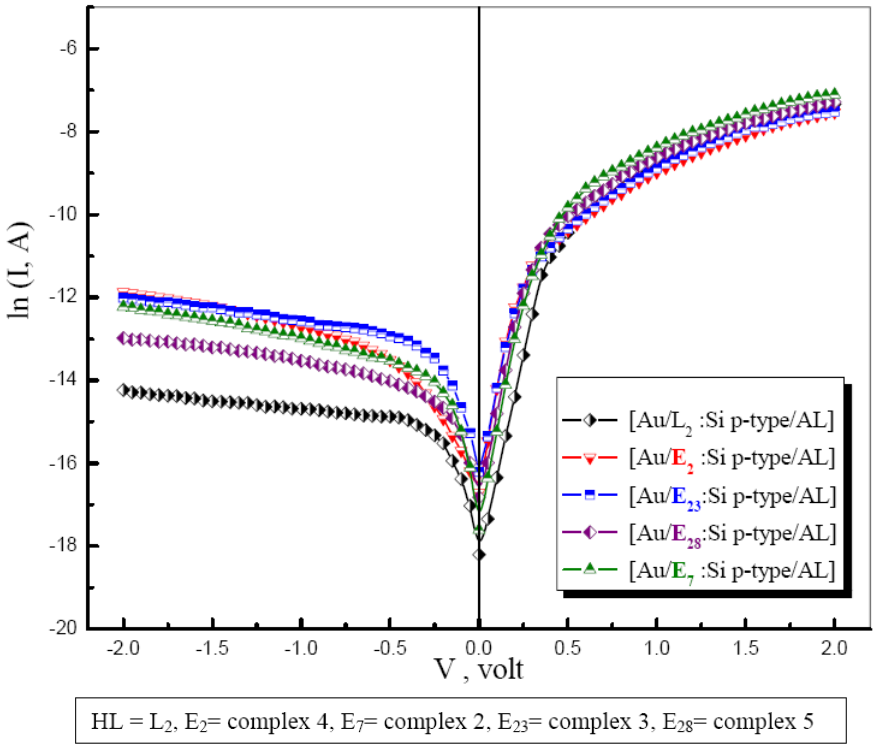

Figure 2. (I–V) characteristics for all prepared devices in forward and reverse conditions.

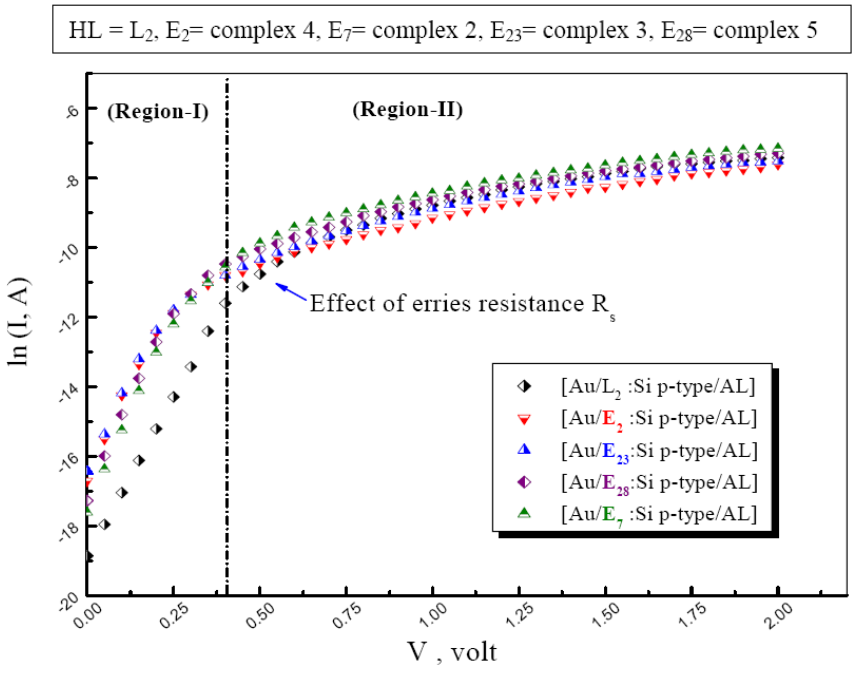

Figure 3. Dark I–V characteristics of the prepared devices at room temperature in forward bias.

The low and weak voltage dependence of the reverse bias current as well as the strong voltage dependence of the forward bias current are characteristic properties of strong rectification performance for the junction diode interface; the RR has been estimated to be 1128 at ±1V at room temperature for Au/E_7:Si p-type/AL as a representative example. The value of the RR is relatively high although the prepared materials are a p-type semiconductor as observed from experiments in our laboratory; this is probably due to the difference in the work functions of p-(synthesized materials) and p-Si as well as the type of conduction in this voltage range [53]. Figure 3 shows the current–voltage (I–V) characteristic observed for the heterojunction under the forward bias for all prepared devices at room temperature. It is obvious that, there is a high series resistance effects at relatively high voltage region $V_F > 0.4$.

When an organic film is inserted between metal and semiconductor, the current–voltage characteristics can be analyzed using the following equation [53,54]:

$$I = I_o \exp\left(\frac{q(V - IR_s)}{nk_BT}\right)\left[1 - \exp\left(-\frac{q(V - IR_s)}{k_BT}\right)\right], \quad (1)$$

$$I_o = AA^*T^2 \exp\left(-\frac{q\Phi_{bo}}{k_BT}\right), \quad (2)$$

where I_o is the reverse saturation current, q is the elementary charge, V is the applied voltage, n is the diode ideality factor, K_b is the Boltzmann's constant, T is the temperature in Kelvin, R_s is the series resistance, A is the effective area and A^* is the effective Richardson constant that takes the value 32 A/cm^2 K^2 for p-Si [55] and Φ_{bo} is the zero-bias barrier height which is expressed as:

$$\Phi_{bo} = \frac{k_BT}{q}\ln\left(\frac{AA^*T^2}{I_o}\right). \quad (3)$$

The value of the ideality factor, n, is calculated from the slope of the linear portion of forward bias of (I–V) characteristic by using the following equation:

$$n = \frac{q}{k_BT}\left[\frac{dV}{d(\ln I)} - IR_s\right]. \quad (4)$$

Under relatively low forward bias condition (V_F < 0.4 V), voltage across the series resistance (IR_s) can be neglected, then, Eq. (4) is simplified to the following equation:

$$n = \frac{q}{k_BT}\left[\frac{dV}{d(\ln I)}\right]. \quad (5)$$

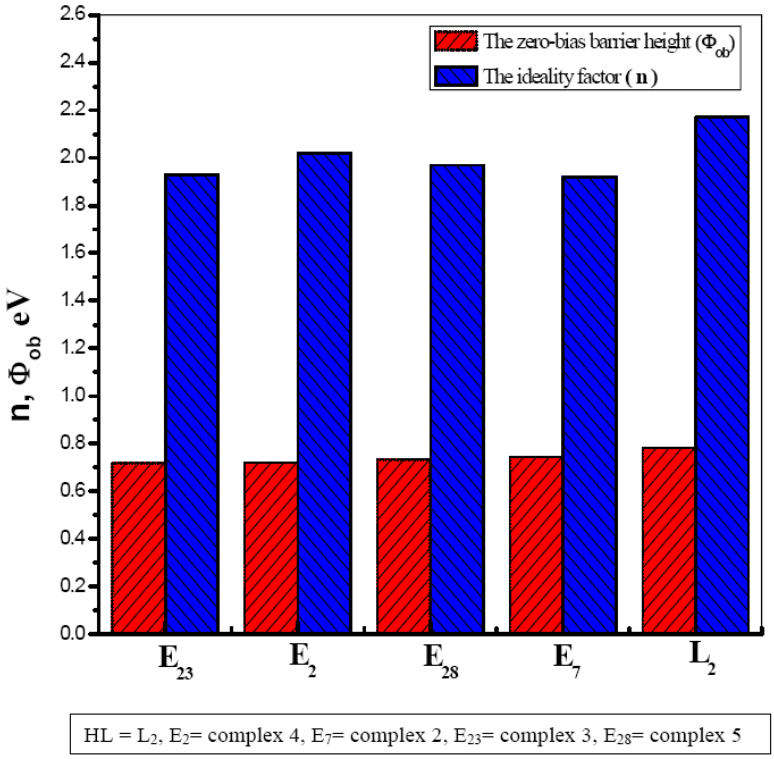

Figure 4. The dependence of the ideality factor, n, and the barrier height, Φ_{ob}, on the nature of the prepared organic material on the p-Si.

By using Eqs. (3) and (5), the experimental values of the Φ_{bo} and the ideality factor, n, for each temperature are determined from the intercept and slope of the relation ln(I) vs. V for forward bias $V_F < 0.4$ V. It should be noted that barrier height the, Φ_{bo}, is the contact barrier that exist at the interface between the organic and the inorganic layers. The heterojunction barrier height controls the injection of charge from the metal/organic contact into the inorganic semiconductor substrate [56]. Figure 4 shows the temperature dependence of n and Φ_{bo} for all devices, from which it can be seen that the values of n and Φ_{bo} depends on the spin coated organic material on the p-Si at the temperature room temperature. The lowest value of n is 1.92 and 1.93 for the prepared materials (complexes (2) and (3)), respectively and the highest one is 2.17 for (HL).The lowest value of the modificated barrier height is 0.721 eV and the ideality factor due to this modification is 2.03 for complex(4). The lowest Φ_{bo} was modificated by (complex(3)) and its value is 0.719 eV and the intermediate value for n and Φ_{bo} is 1.97 and 0.734 eV for (complex(5)). The previous investigated results reveal that the prepared dye and its metal complexes can play rules in the modification of the barrier height of the heterojunctions to control the injection of charges from the metal/dye contact into the p-Si/Al in electronic applications [57, 58]. Boyarbay et al. [59] reported that although the standard thermionic emission assumes the barrier height is independent of the temperature; this result confirms that the Reactions of HL with metals have the ability to modificate the barrier height of the fabricated devices and also the noticed different values of the ideality factor may be returned to the nature of the prepared dyes. All the fabricated devices are investigated at the

room temperature 293 K and the temperature dependence of the ideality factor and the barrier height not include in our study.

In the relative higher voltage region, $V_F > 0.5$ V, the concave deviation from straight line is caused by the presence of the interface states and the series resistance, R_s, associated with bulk Si and the ohmic contacts. The series resistance is a very important parameter of the heterojunction. When the applied voltage is sufficiently large, the ideality factor and the series resistance were evaluated using a method developed by Cheung and Cheung [60]. The Cheung's method is achieved by using Eq. (1) in the following form [55]:

$$V = IR_s + n\Phi_{bo} + n\frac{k_BT}{q}\ln\left(\frac{I}{AA^*T^2}\right), \tag{6}$$

$$\frac{dV}{d(\ln\ I)} = \frac{nk_BT}{q} + IR_s, \tag{7}$$

$$H(I) = V - n\frac{k_BT}{q}\ln\left(\frac{I}{AA^*T^2}\right), \tag{8}$$

$$H(I) = IR_s + n\Phi_{bo}. \tag{9}$$

Figure 5 shows the plot of [dV/d(ln I)] vs. I. The slope of the linear fit gives the series resistance while its intercept gives the ideality factor at room temperature. The temperature dependence of the series resistance and the ideality factor values are given inset Figure 5. Using Eq. (7), the values of Φ_{bo} and Rs were calculated at different temperatures from the relation between H(I) and I and given inset Figure 6.

Nord proposed an alternative method to determine the series resistance and the barrier height [61]. The following functions have been defined in the modified Nord's method [55,61] which applied to the full forward bias region of the I–V characteristics of the junction:

$$F(V) = \frac{V}{\gamma} - \frac{k_BT}{q}\left(\frac{I}{AA^*T^2}\right), \tag{10}$$

where γ is the first integer (dimensionless) greater than n which obtained from I–V measurements, here it has been taken as 3. In this function the barrier height can be obtained by using the following equation [55,61]:

$$\phi_b = F(V_o) + \frac{V_o}{\gamma} - \frac{k_BT}{q}, \tag{11}$$

where $F(V_o)$ is the minimum F(V) value of Nord's function of F(V) vs. graph and V_o is the

corresponding voltage. Figure 7 shows the voltage dependence of F(V) at different temperatures. Also, the series resistance, Rs, can be calculated from Nord's functions as [55,61]:

$$R_S = \frac{k_B T(\gamma - n)}{qI}. \tag{12}$$

The values of the barrier height and the series resistance at different temperatures were obtained using Eqs. (9) and (10) and listed inset Figure 7.

The discrepancy between the values of the series resistance and the barrier height obtained from Cheung's functions and Nord's functions may be due to the Cheung's function applied only for the nonlinear region of forward bias while Nord's function are applied for the whole forward bias region of I–V curve [55].

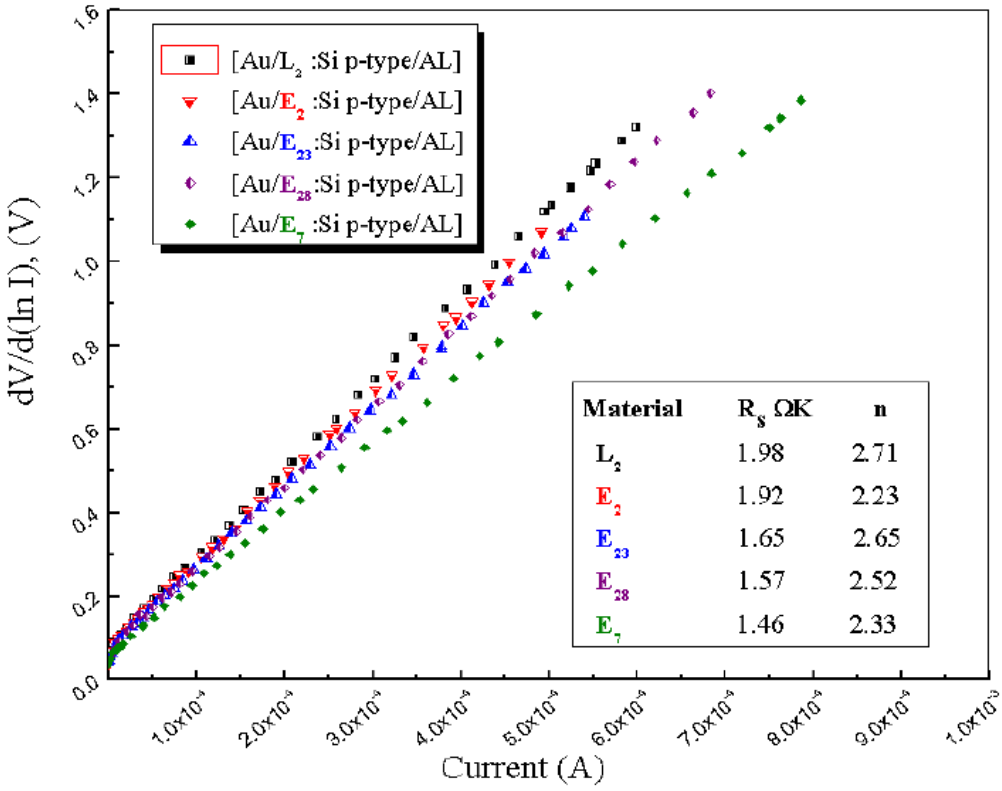

Figure 5. Plot of [dV/d(ln I)] vs. I at room temperature. The inset table indicates the investigated values of the ideality factor, n, and series resistance, R_s, for all fabricated organic dyes/p-Si heterojunctions.

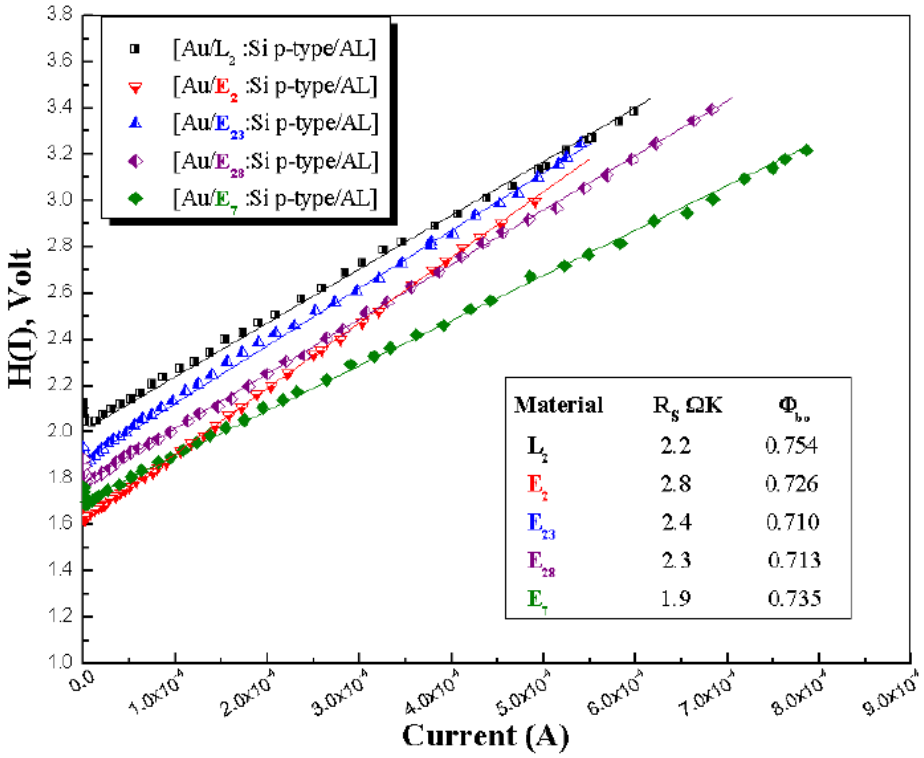

Figure 6. Plot of H(I) and I at room temperature 293 K. The inset table data the investigated values of the barrier height, Φ_{ob}, and series resistance, R_s, for all fabricated organic dyes/p-Si heterojunctions.

3.4. Photovoltaic Response of the Au/Synthesized-Dyes/P-Si/Al Device

All the prepared heterojunctions by using the pre-prepared organic dyes showed an initial response under illumination. This response depends on the inserted organic layer between the (Au) as an ohmic contact for the inserted organic layer (HL, complex(4), complex(3), complex(5) or complex(2)) and the p-Si as an inorganic semiconductor, the injection of charge is controlled by the inserted organic layer as the I–V characteristic curves (in dark and under illumination) reveals in Figure 8. All the prepared devices have the same active area (0.06 cm^2) and investigated under the same conditions of illumination and with the white light of power 6 mW/cm^2. For each device, it can be seen that at a certain voltage, the current value for each cell under illumination is higher than in the dark condition; this phenomenon is a result of the difference in the electron affinities of the two semiconductors [62,63].

All (I–V) characteristic curves of maximum power region for the prepared heterojunctions with the different synthesized organic dyes are collected in one master diagram as shown in Figure 9(a). On illumination, the light generates a photocurrent and its influence appears in the region of the fourth quadratic, which is plotted separately in the previous figure.

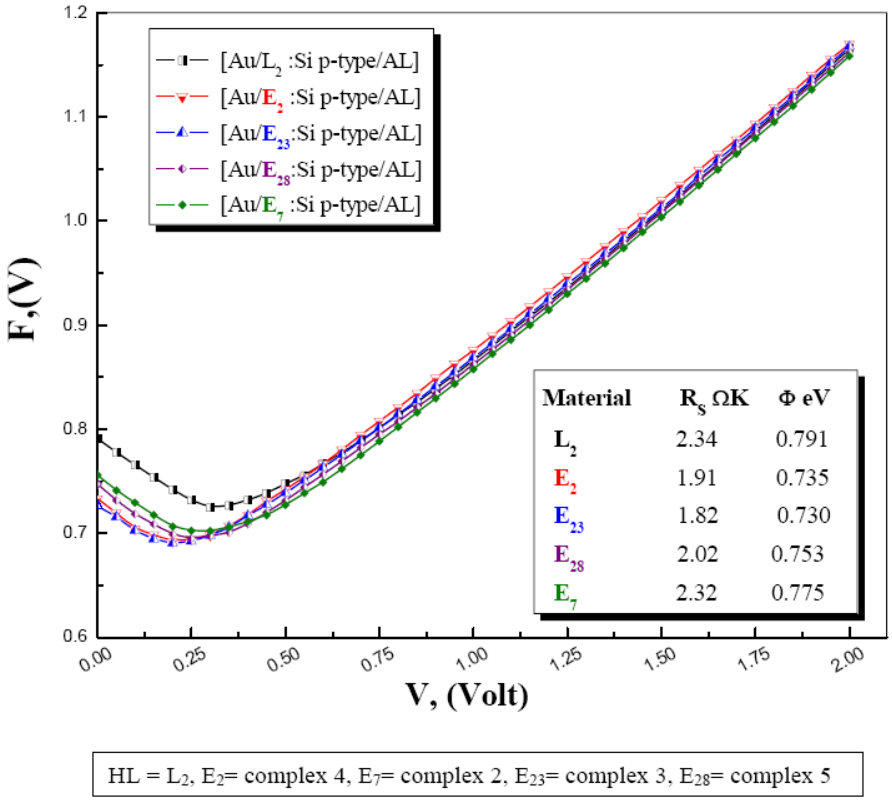

Figure 7. Voltage dependence of F(V) at room temperature 293. The inset table data the investigated values of the barrier height and series resistance by using Nord's method for all fabricated organic dyes/p-Si heterojunctions.

Table 5. Summary of surface morphology parameters from AFM image analyses

Roughness Parameter	Complex(2) thin film category	
	Spin-coated (2) on p/Si/Al at 293 K	Annealed (2)/p-Si/Al at 253 K
R_q (nm) Root Mean Square (RMS) parameter	6.23	4.78
$R_{(p-v)}$ (nm) Mean peak-to-valley profile roughness	39.7	31
R_v (nm) Maximum Valley Depth	12.24	8.86
R_p (nm) Maximum Peak Height	27.43	22.13
Projected area (μm²)	0.25	0.25
S_{hw} (nm) Mean Half Wavelength	262.2	196.2

All the prepared devices exhibit a short circuit current, I_{sc}, and an open-circuit voltage, V_{oc}. The variation in the resultant values of (I_{sc}) and (V_{oc}) confirms the modification of the charge injection from the metal/organic into the p-Si substrate and depicts that the barrier height is controlled by the inserted organic layer under the same conditions of preparation and

measurements. The photovoltaic parameters for each device are investigated and recorded in Table 2. The photoresponsivity value for the heterojunction is defined as the ratio of photocurrent to dark current (I_{photo}/I_{dark}) [63].

As seen in the previous figure, the photoresponsivity of the heterojunction under light illumination due to the photogeneration of charges carriers. The prepared heterojunctions exhibit a different photosensitivity under visible light illumination of 6 mW/cm^2. It is observed that the photocurrent in the device in reverse direction is strongly enhanced by photo-illumination.

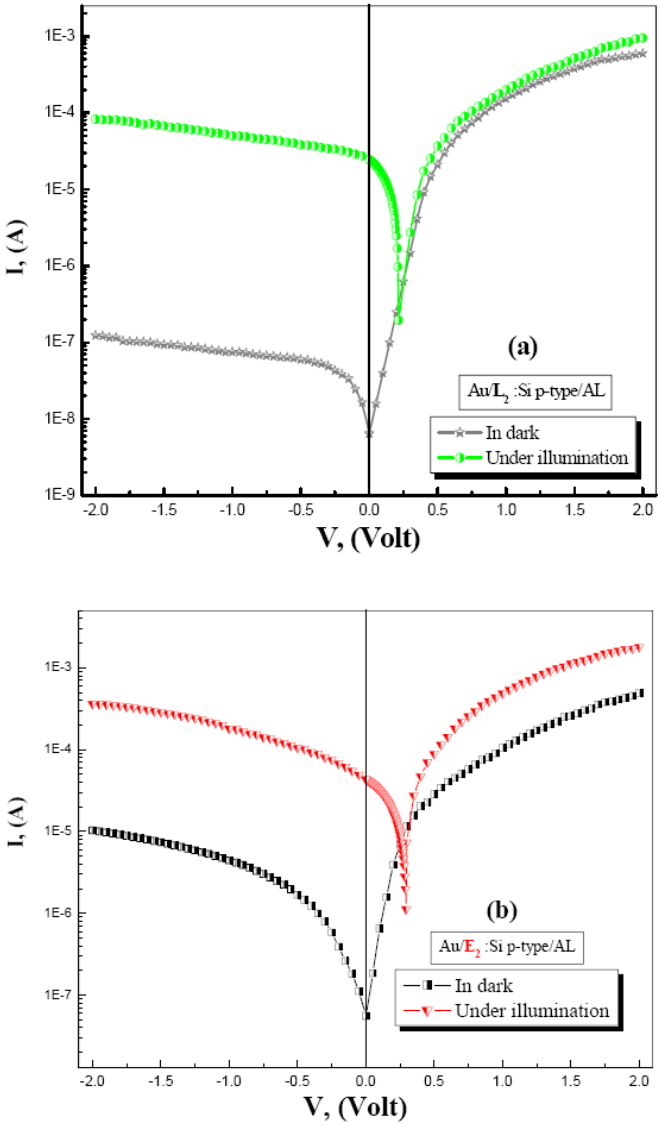

Figure 8. (Continued).

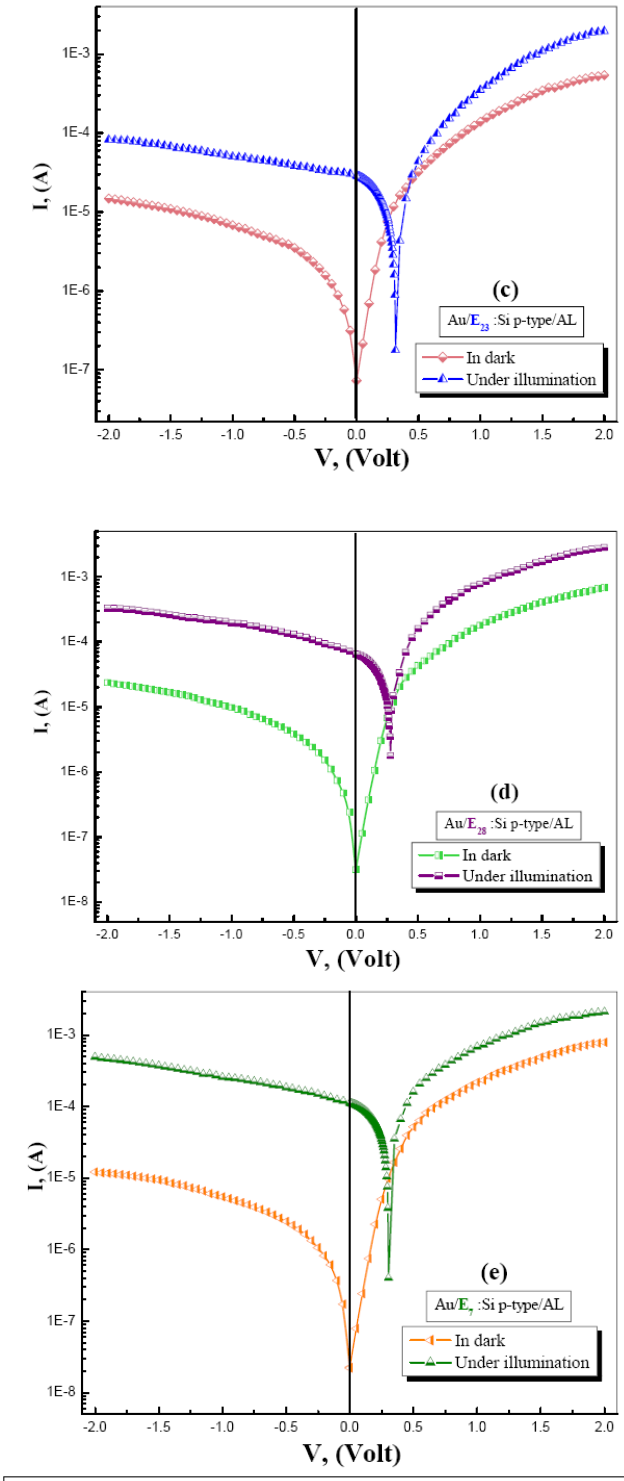

Figure 8. (I–V) characteristic curves for Au/p-DOPNA/p-Si/Al heterojunction diode under dark and illumination conditions measured at room temperature.

This behavior yields useful information on the electron–hole pairs, which were effectively generated in the junction by incident photons. Under the influence of the electric field at the junction, the free electrons and holes were accelerated towards the Au and Al electrodes along the potential barrier at the interface [64]. Figure 9(b) is introduced as a representative sample (Au/complex(2):Si p-type/AL) of the best resultant device of the maximum power region.

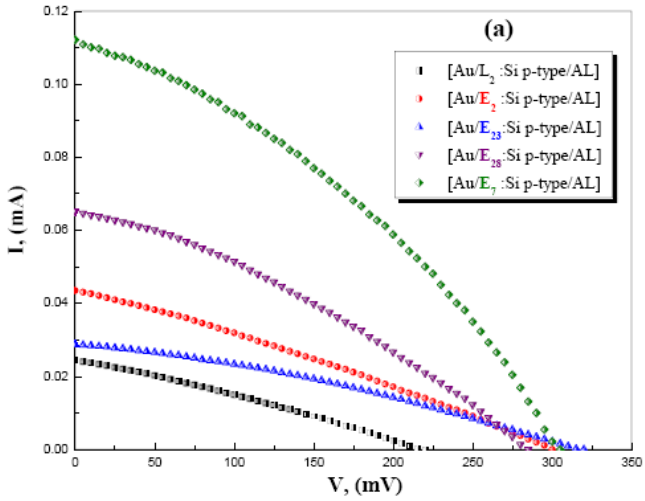

HL = L_2, E_2= complex 4, E_7= complex 2, E_{23}= complex 3, E_{28}= complex 5

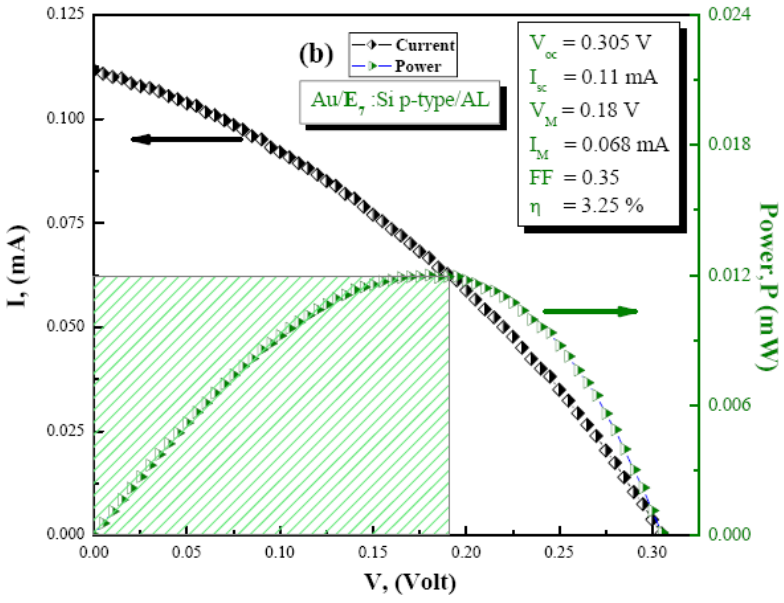

Figure 9. Loaded I–V characteristic and power of (a) all fabricated Au/org-dye:p-Si/Al heterojunction and (b) Au/E_7:p-Si/Al heterojunction under illumination as a representative sample.

As can be seen, the values of the open circuit voltage, Voc, the short-circuit current, Isc, voltage at maximum power point, VM, and the current at maximum power point, IM, for the device were obtained as 0.305 V, 0.11 mA, 0.175 V and 0.068 mA, respectively. The FF is given by [65]

$$FF = V_M I_M / V_{oc} I_{sc} \quad (13)$$

The value of the FF was calculated as 0.35. The experimental power conversion efficiency of a solar cell is given by [65]

$$\eta = (FFV_{oc}I_{sc})/AP_{in} \times 100\ \% \quad (14)$$

where P_{in} is the illumination intensity impinging on the cell and A the effective area. The efficiency of the cell was calculated as 3.3 %. The fill factor value of complex(2)/p-Si device, like some other organic based devices, is lower in comparison to those of solar cells based on inorganic materials. The main reason of this result can be attributed to the field dependent nature of the charge photogeneration process or high series resistance of the organic layer [7]. Therefore, it can be said that the complex(2)/p-Si heterojunction has a good photovoltaic parameters and 2-Aminothiazoles and their derivative-dyes which may be alternative candidate for photovoltaic application based on organic molecules. Moreover, as observed from the above comparative study, the presented devices exhibit considerably acceptable photovoltaic properties valid for photovoltaic sensor applications, especially when the reproducibility phenomenon was taken into consideration.

The low hole mobility, the disordered dissociation and charge dissipated recombination in organic materials lead to both lower efficiency and fill factor [66].

Table 6. Photovoltaic parameters of some organic ligand and complex heterojunction solar cells

Solar cell construction	J_{sc} (mA/cm^2)	V_{oc} (V)	Fill factor	Efficiency (%)	Ref.
Au/HL :Si p-type/AL	4.1×10^{-4}	0.215	0.29	4.26×10^{-4}	Present Work
Au/(4) :Si p-type/AL	7.3×10^{-4}	0.3	0.28	1.02×10^{-3}	
Au/(3):Si p-type/AL	0.48	0.315	0.33	0.83	
Au/(5):Si p-type/AL	1.1×10^{-3}	0.285	0.32	1.65×10^{-3}	
Au/(2) :Si p-type/AL	1.86	0.305	0.35	3.3	
Al/TPP/Au	–	0.74	0.18	0.06	[67]
Au/Ni-phthalocyanine/p-Si/Al	3.67	0.35	0.4	1.05	[68]
Ag/p-CuPc/n-GaAs/Ag	0.072	0.20	0.22	2.9×10^{-3}	[69]
pentacene/n-Si photovoltaic device	0.471	0.22	0.42	0.044	[70]
Au/PYR(G)/p-Si/Al	0.72	0.50	0.41	1.44	[7]

CONCLUSION

2-Acetylamino-5-phenylazo-thiazole (HL) and its complexes with Cu(II), Co(II), Ni(II) and Fe(III) have been prepared and characterized . The obtained data show that the reaction of

ligand with metal ions led to the formation of 1:1 metal complexes as in case of Cu(II) and Co(II) ,whereas, in case of Ni(II) and Fe(III) 1:2 (metal: ligand) complexes were formed. The results also show that in Cu(II) complex, the ligand behaves as a monobasic tridentate ligand coordinating via the azo nitrogen atom, sulfur atom and the enolic oxygen atom (NSO mode).Whereas, in case of complexes of Co(II), Ni(II) and Fe(III), the ligand behaves as a neutral bidentate, coordinating through the azo nitrogen and sulfur atoms (NS mode).

The analysis of the AFM topological image showed a large scale of nano particles. The current–voltage (I–V) characteristics of the Au/synthesized-dye/p- Si/Al heterojunction have been measured at the room temperature 293 °K. The effect of the synthesized dye and its complexes on the heterojunction parameters as Φ_{ob}, n and R_s, were determined from I–V measurements with considering the inhomogeniety due to the mismatch through the spin-coated dye/p-Si interface. The synthesized dye and its metal complexes modified the ideality factors and barrier heights at room temperature. The dominant operating mechanism in the reverse bias is generation recombination of carriers, which is limited to the process of powder, spin-coated dye on the p-Si and annealing temperature at 353 °K. The investigation of (I–V) characteristics under illumination of =6 mW/cm^2 confirms that the short-circuit current, I_{sc}, is open-circuit voltage, V_{oc}, and the fill factor, FF, are depending on the synthesized dyes. From the extracted experimental data, The fabricated device; Au/complex(2):p-Si/Al is the best one as photovoltaic device with conversion efficiency equal to 3.3 %. Its short-circuit current, I_{sc}, is open-circuit voltage, V_{oc}, and the fill factor, FF, are 0.11 mA, 0.305 V and 0.35%, respectively. The obtained results have suggested the fabricated heterojunction is a potential candidate for photovoltaic sensor application.

ACKNOWLEDGMENTS

Thanks are due to Scientific Research Deanship, Qassim University, KSA, for financial supporting this work (Research project number 798).

The author do their appreciation to professors; M.M. El-Nahass and H.M. Abd El-Khalek, for their help for organic/inorganic heterojunction part.

REFERENCES

[1] Y.-J. Liu and H.-Z. Yu, *J. Phys. Chem.* B. 107 (2003) 7803.

[2] H. Haick, M. Ambrico, T. Ligonzo, R.T. Tung, D. Cahen and *J. Am. Chem. Soc*. 128 (2006) 6854.

[3] Aviram and M.A. Ratner (Eds.), Molecular Electronics: Science and Technology, *Ann. N.Y. Acad. Sci.*, (1998).

[4] Vilan, A. Shanzer and D. Cahen, *Nature* 404 (2000) 166.

[5] M.M. El-Nahass, A.F. El-Deeb, H.S. Metwally and A.M. Hassanien, *Materials Chemistry and Physics 125* (2011) 247.

[6] M.M. El-Nahass, H.S. Metwally, H.E.A. El-Sayed and A.M. Hassanien, *Synthetic Metals* 161 (2011) 2253.

[7] A.A.M. Farag, H.S. Soliman and A.A. *Atta, Synthetic Metals* 161 (2012) 2759.

[8] M.E. Aydin, A.A.M. Farag, M. Abdel-Rafea, A.H. Ammar and F. Yakuphanoglu, *Synthetic Metals 161* (2012) 2700.
[9] El Amrani, B. Lucas and B. Ratier, *Synthetic Metals* 161 (2012) 2566.
[10] L. G. Kaake, P. F. Barbara, and X.-Y. Zhu, *J. Phys. Chem. Lett.* 1(2010) 628.
[11] D.Y. Kim, J. Subbiah, G. Sarasqueta, F. So, H. Ding, Irfan and Y. Gao, *Appl. Phys. Lett.* 95 (2009) 093304-1–093304-3.
[12] Friedel, P.E. Keivanidis, T.J.K. Brenner, A. Abrusci, C.R. McNeill, R.H. Friend and N.C. Greenham, *Macromolecules* 42 (2009) 6741.
[13] H. Beyer, Organic Chemistry, Verlag Harry Deutsch, *Frankfurt-um-Main and Zürich*, 1963, pp. 609.
[14] A.-C. Gaumont, M. Gulea and J. Levillain, *Chem. Rev*. 109 (2009) 1371.
[15] U.G. Ibatullin, T.F. Petrushina, L.Y. Leitis, I.Z. Minibaev, B.O. Logvin, Khim. Geterotsitl. *Soedin*. (1993) 715.
[16] P.C. Hang and J.F. Honek, Bioorg. *Med. Chem. Lett.* 15 (2005) 1471.
[17] P. Beuchet, M. Varache-Lembège, A. Neveu, J.-M. Léger, J. Vercauteren, S. Larrouture, G. Deffieux, A. Nuhrich, *Eur. J. Med. Chem.* 34 (1999) 773.
[18] Geronikaki, P. Vicini, N. Dabarakis, A. Lagunin, V. Poroikov, J. Dearden, H. Modarresi, M. Hewitt and G. Theophilidis, *Eur. J. Med. Chem*. 44 (2009) 473.
[19] Papadopoulou, A. Geronikaki and D. Hadjipavlou-Litina, *Farmaco* 60 (2005) 969.
[20] Kreutzberger and H. Schimmelpfennig, *Arch. Pharm*. 314 (1981) 385.
[21] Keil, R. Flaig, A. Schroeder and H. Hartmann, Dyes Pigments 50 (1) (2001) 67.
[22] M.A. Metwally, E. Abdel-latif, A.M. Khalil, F.A. Amer and G. Kaupp, *Dyes Pigments* 62 (2) (2004) 181.
[23] K. Singh, S. Singh and J.A. Taylor, *Dyes Pigments* 54 (3) (2002) 189.
[24] M.S. Yen and I.J. Wang, *Dyes Pigments* 67 (3) (2005) 183.
[25] Y. Geng, D. Gu, F. Gan, *Optical Materials*, 27 (2004) 193.
[26] W. Bin, W. Yi-Qun, G. Dong-Hong, G. Fu-Xi, *Chinese Physics Letters*, 20 (2003) 1596.
[27] H. Fu-Xin, W. Yi-Qun, G.Dong-Hong, G. Fu-Xi, *Chinese Physics Letters*, 20 (2003) 2259.
[28] E. Hamada, T. Fujii, Y. Tomizawa, S. Limura, *Japanese Journal of Applied Physics*, 36 (1997) 593.
[29] Y. Suzuki, Y. Okamoto, Y. Kurose, S. Maeda, *Japanese Journal of Applied Physics*, 38 (1999) 1669.
[30] E. Radziemska, *Energy Convers. Manag*. 46 (2005) 1485.
[31] V. Badescu, *Energy Convers. Manag*. 47 (2006) 1146.
[32] K. Bouzidi, M. Chegaar and A. Bouhemadou, *Sol. Energy Mater. Sol*. Cell 91 (2007) 1647.
[33] Z. Zhou, K. Zhao, *Energy Convers. Manag*. 52 (2011) 2153.
[34] M. Ramadan, I. M. EL-Mehasseb. *Trans. Met. Chem*. 23 (1998) 183.
[35] E. W. Ainscough, A. M. Brodie, A. J. Dobbs, J. D. Ranford, J. M. Waters, *Inorg. Chem*. *Acta* 267 (1998) 27.
[36] M.M. El-Nahass, H.M. Abd El-Khalek and Ahmed M. Nawar, *Optics Communications*, 285 (2012)1872.
[37] M.M. El-Nahass, H.M. Abd El-Khalek and Ahmed M. Nawar, *Eur. Phys. J. Appl. Phys.* (2012) DOI: 10.1051/epjap/2012110280.

[38] M.M. El-Nahass, A. A. Atta, H. E. A. El-Sayed and E. F. M. El-Zaidia, current organic chemistry, *ISSN*:13852728(2010)1.
[39] W. J. Geaey, *Coord. Chem. Rev*.7 (1971) 81.
[40] N.N. Greenwood, B.P. Straughan, A.E. Wilson, *J. Chem. Soc. A* (1968) 2209.
[41] A.S. El-Tabl, F.A. El-Saied and A.N. Al-Hakimi ,*Transition Met. Chem*. ,32 (2007) 689
[42] M. Teotia, J.N. Gurthu, V.B. Rama, *J. Inorg. Nucl. Chem*. 42 (1980) 821
[43] K.B. Gudasi, S.A. Patel, R.S. Vadvavi, R.V. Shenoy, M. Nethaji, *Trans. Met. Chem.*, 586 (2006) 31.
[44] El-Motaleb, M. Ramada, W. Sawodny, H.F. El-Baradie, M. Gaber, *Trans. Met. Chem*., 211 (1997) 22.
[45] P. Lever, Inorganic Electronic Spectroscopy, Second edition, *Elsevier Science Publishing Company*, Amsterdam, 1984.
[46] Labadi, L. Horvath, G. Liptay, *J. Therm. Anal. Cal*. 83, (1) (2006) 247.
[47] Cukurovali, I. Yilmaz, *Trans. Met. Chem.* 31 (2006) 207.
[48] D.X. West, L.K. Pannell, *Trans. Met. Chem*. 14 (1989) 457.
[49] P.K. Singh, D.N. Kumar, *Spectrochim. Acta, Part A* 64 (2006) 853.
[50] B. P. Lever "Inorganic Electronic Spectroscopy" *El-Sevier Amsterdam* (1968).
[51] M.A. Ali, A.H. Mirza, C.Y. Yee, H. Rahgeni, P.V. Bernhardt; *Polyhedron* 30 (2011) 542–548
[52] A.S. El-Tabl, M.M. E. Shakdofa, A. M.A. El-Seidy, Ahmed N. Al-Hakimi, *J. Korean Chem. Soc.* 2011, Vol. 55,19-27.
[53] K.R. Rajesh and C.S. Menon, *J. Non-Cryst. Solids* 353 (2007) 398.
[54] S.M. Sze and K.K. Ng, Physics of Semiconductors Devices, 3rd ed., *John Wiley and Sons, Inc*., Hoboken, NJ, 2007.
[55] N. Kavasoglu, C. Tozlu, O. Pakma, A.S. Kavasoglu, S. Ozden, B. Metin, O. Birgi and S. Oktik, *Synthetic Met*. 159 (2009) 1880.
[56] Temirci, M. C¸ akar, A. Türüt and Y. Onganer, *Phys. Status Solidi* (a) 201 (2004) 3077.
[57] Dietrich R.T. Zahn, Sunggook Park and Thorsten U. Kampen, *Vacuum* 67 (2002) 101.
[58] M. Fahlman and W.R. Salaneck, *Surface Science* 500 (2002) 904.
[59] Boyarbay, H. C¸ etin, A. Uygun and E. Ayyildiz, *Thin Solid Films* 518 (2010) 2216.
[60] S.K. Cheung and N.W. Cheung, *Appl. Phys. Lett*. 49 (1986) 85.
[61] H. Nord, *J. Appl. Phys.* 50 (1979) 5052.
[62] M.M. El-Nahass, A.M. Farid and A.A.M. Farag, H.A.M. Ali, *Vacuum* 81 (2006) 8.
[63] F. Yakuphanoglua and W.A. Farooq, *Synth. Met.* 161 (2011) 379.
[64] G.D. Sharma, S.K. Gupta and M.S. Roy, *Thin Solid Films* 333 (1998) 176.
[65] H.M. Zeyada, M.M.El-Nahass and E.M.El-Menyawy, *Solar Energy Materials and Solar Cells* 92 (2008) 1586.
[66] W. Hu, M. Matsumura, *J. Phys., D Appl. Phys*. 37 (2004) 1434.
[67] K. Takahashi, S. Nakatani, T. Yamaguchi, T. Komura, S. Ito, K. Murata, *Sol. Energy Mater. Sol. Cell* 45 (1997) 12.
[68] S. Riad, *Thin Solid Films* 370 (2000) 253.
[69] Kh.S. Karimov, M.M. Ahmed, S.A. Moiz, M.I. Fedorov, *Sol. Energy Mater. Sol. Cells* 87 (2005) 61.
[70] N. Oyama, Y. Takanashi, S. Kaneko, K. Momiyama, K. Suzuki and F. Hirose, *Microelectronic Engineering* 88 (2011) 2959.

Smart Nanocomposites
Volume 3, Number 1
ISSN: 1949-4823

SYNTHESIS AND OPTICAL PROPERTIES OF RARE-EARTH AND TRANSITION METALS DOPED TITANIUM DIOXIDE FILMS

Y. V. Gerasimenko*, V. A. Logacheva and A. M. Khoviv
Voronezh State University, Voronezh, Russia

ABSTRACT

In this paper we report the formation and investigation of a series of titanium dioxide films doped by rare-earth and transition metals. M/TiO_2/Si(or quartz) (M = La, Sm, Ni, Co) two-layers structures were prepared using magnetron and high-frequency plasma sputtering. Subsequent thermal treatment and pulse photon annealing resulted in the formation of compound oxide films consisting of $La_2(TiO_3)_3$ and La_2TiO_5, Sm_2TiO_5, $NiTiO_3$, $CoTiO_3$. Comparing with initial TiO_2 short-wave transmission, the edge of energy band shifted. La and Sm dopants shift this edge to short-wave region, while Ni and Co dopant - to long-wave region. The corresponding analysis of edge absorption and transition energy values determination is presented.

Keywords: thin films; titanium dioxide; compound oxide; doping; magnetron sputtering; high-frequency plasma sputtering; oxidation; absorption spectroscopy

INTRODUCTION

Thin-film optical coatings are regarded as potential surface materials for science, power engineering, medicine, etc. One of the most significant scopes of antireflection coatings is the solar power engineering [1, 2]. Principal factor influencing coatings quality and in the case of vacuum technological processes is the factor of a composition and a quality of the film-forming materials used for deposition of optical coatings [3]. The list of materials applicable to manufacture of thin-film coatings is large. Equally with single-component materials (TiO_2, ZrO_2, HO_2, SiO_2) the increasing application is found by mixes of substances and solid solutions on their basis [4].

New composite materials based on titanium dioxide are of the greatest interest. Titanium dioxide films are used in photovoltaics as antireflection coatings due to their excellent optical

* E-mail: yuliya-gerasimenko@yandex.ru

properties, chemical resistance, thermal stability [5, 6]. Doping of rare-earth and transition metals allow to improve optical properties, mechanical and exploitation stability of TiO_2 [7].

In addition, rare-earth and transition metals doping is required for luminescent properties. The luminescence of optical coatings increases the efficiency of photovoltaics.

EXPERIMENTAL DETAILS

Doped titanium dioxide nanocrystalline films (*M*:TiO_2; *M* = La, Sm, Co, Ni) were successfully synthesized by thermal oxidation and pulse photon annealing of two-layers structures: La/TiO_2/Si(quartz), Sm/TiO_2/Si(quartz), Ni/TiO_2/Si(quartz), Co/TiO_2/Si(quartz) on silica and quartz substrates.

TiO_2 has been deposited by two different techniques, including magnetron sputtering with subsequent thermal oxidation at 723 K and high-frequency plasma sputtering. The next step was the magnetron sputtering of doping metal (M = La, Sm, Ni, Co) with subsequent thermal oxidation at following temperatures: T = 723, 873 and 1023 K and pulse photon annealing. The result of this synthesis was formation of the compound oxide films with thickness ~ 300 nm.

Metal films were deposited on quartz and silicon (100) substrates by magnetron sputtering from a metallic targets (Ti, La, Sm, Ni, Co) (99.8 % purity) in a vacuum chamber (pressure $6 \cdot 10^{-6}$ Torr). Experimental conditions were as follows: the deposition occurred in atmosphere of high purity (99.9997 %) argon (partial pressure $2 \cdot 10^{-3}$ Torr), current 0.5 A for Ti, 0.2 A for La and Sm, 0.5 A for Ni and 0.7 for Co. Thickness were determined by the deposition time.

Titanium dioxide films were also deposited by reactive r. f. sputtering technique from a metallic titanium target (99.8 % purity) in atmosphere of high purity (99.98 %) oxygen as a reactive gas (partial pressure $4.5 \cdot 10^{-2}$ Torr), and argon (99.9997 % purity) as a sputtering gas (partial pressure $9.5 \cdot 10^{-2}$ Torr). Monocrystalline silicon and quartz were used as the substrates and their temperature during deposition was maintained at 400 K. Thickness were determined by the deposition time.

The crystalline structures of the films were measured using X-ray diffraction (XRD) with Cu Kα source (Thermo Scientific ARL X'TRA with ICDD data). SEM (Jeol JSM-6510LV) was used for the surface investigations and thickness measurements of the films. Optical transmittance of films was measured at room temperature with Shimadzu UV-2550 spectrophotometer, using the substrate properties as background references. The photoluminescence emission spectra were recorded with spectral luminescent complex using laser (λ = 337 nm) for photoluminescence excitation at the liquid-nitrogen temperature.

RESULTS AND DISCUSSION

It has been established that during thermal treatment process of two-layers structures M/TiO_2/Si(quartz) the compound oxide films with thickness 300 nm consisting of $La_2(TiO_3)_3$ and La_2TiO_5, Sm_2TiO_5, $NiTiO_3$, $CoTiO_3$ respectively for each structure has been generated. X-ray diffraction patterns and SEM images of this structures are shown in Figure 1 – Figure 4.

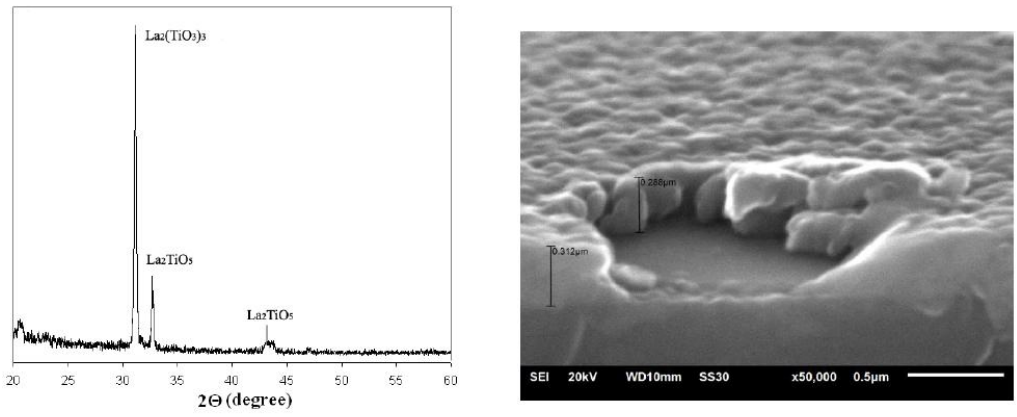

a b

Figure 1. X-ray diffraction pattern (a) and SEM image (b) of the La/TiO_2/Si structure after pulse photon annealing.

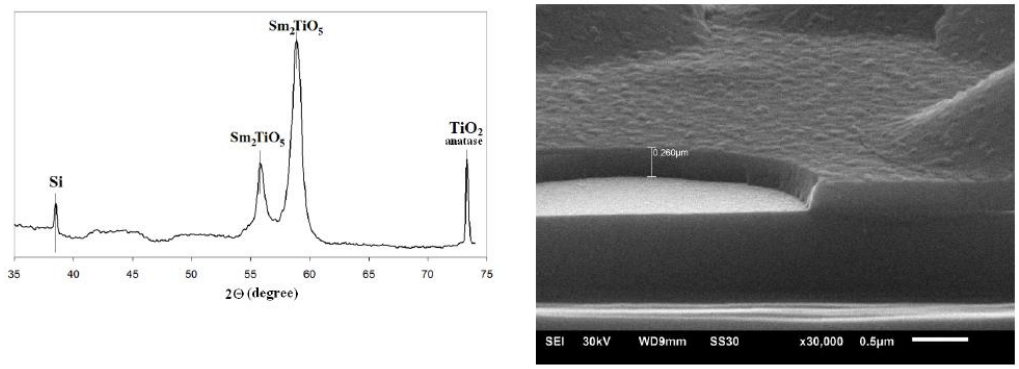

a b

Figure 2. X-ray diffraction pattern (a) and SEM image (b) of the Sm/TiO_2/Si structure after thermal oxidation at T = 1023 K.

The transmittance of films deposited on clear quartz was measured over the range of 200 to 900 nm. Figure 5 shows the optical transmittance spectra of thin films TiO_2/quartz and *M*:TiO_2/quartz, *M* = La, Sm, Co, Ni. Absorption spectroscopy shows that TiO_2 film has high transparency in the wavelength range from 350 to 900 nm and absorption band at spectral range from 190 to 350 nm. The transmittance of the TiO_2 film was about 90 %.

Metal used for doping determines the shift of short-wave transmission band edge and the optical transition energy. The films transmission increases through the doping of impurity atoms. For TiO_2 the short-wave edge wavelength is equal to 350 nm, La and Sm doping shift this edge to short-wave region and the edge wavelength becomes 330 and 270 nm respectively. Ni and Co doping shifts this edge to long-wave region and the edge wavelength es to 355 and 370 nm respectively.

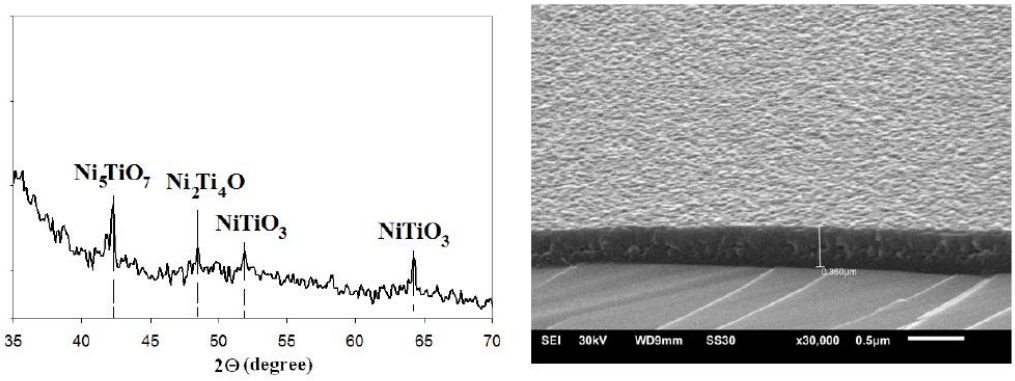

a b

Figure 3. X-ray diffraction pattern (a) and SEM image (b) of the $Ni/TiO_2/Si$ structure after thermal oxidation at T = 1023 K.

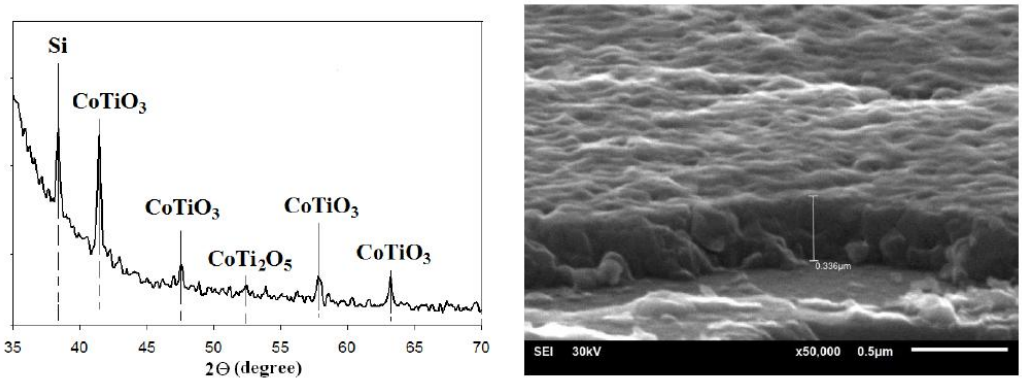

a b

Figure 4. X-ray diffraction pattern (a) and SEM image (b) of the $Co/TiO_2/Si$ structure after thermal oxidation at T = 1023 K.

The optical band gap energy for the thin films was determined from the sharply falling transmission region, using Tauc's low [8]. The analysis of edge absorption has shown that transition energy value is 3.67 eV for TiO_2. The optical transition energy was 3.70 and 3.06 eV and correspond to $La_2(TiO_3)_3$ and La_2TiO_5 respectively, 4.7 eV for Sm_2TiO_5, 3.64 eV for $NiTiO_3$ and 3.35 eV for $CoTiO_3$.

Photoluminescence emission spectra of thin films M:TiO_2/quartz, M = La, Sm, Co, NI are shown in Figure 6. Shapes of the spectra are quite similar, but they differ in the intensity of the bands.

The luminescence band of thin films M:TiO_2 is wide and it's located in the region from 420 nm to 850 nm with maximum at 550 nm. Samarium doped titanium dioxide film has the most high intensity and complementary luminescence band with maximum at 830 nm.

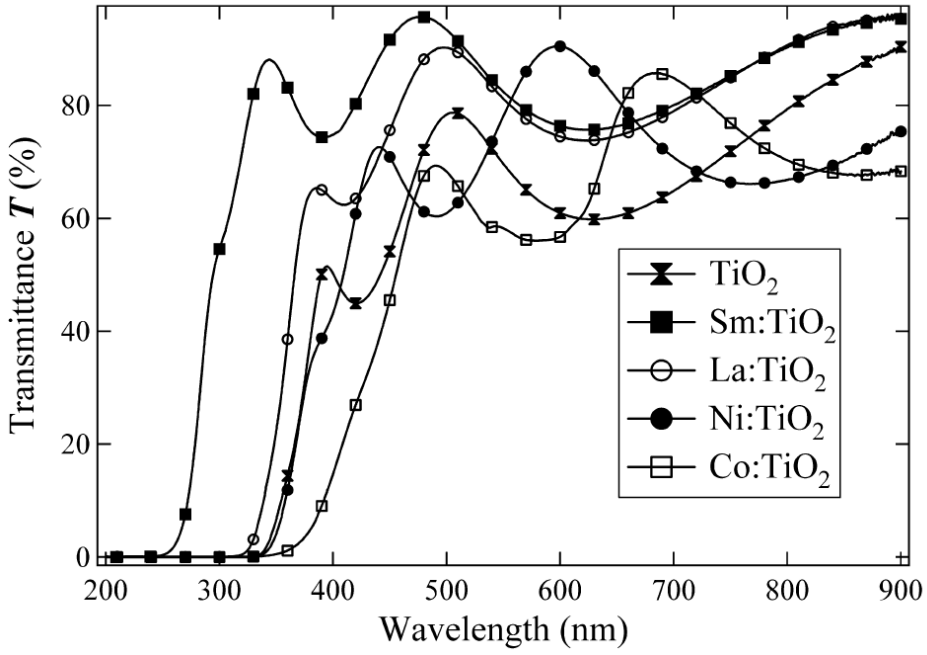

Figure 5. Optical transmittance T spectra of thin films TiO2/quartz and M:TiO2/quartz, M = La, Sm, Ni, Co.

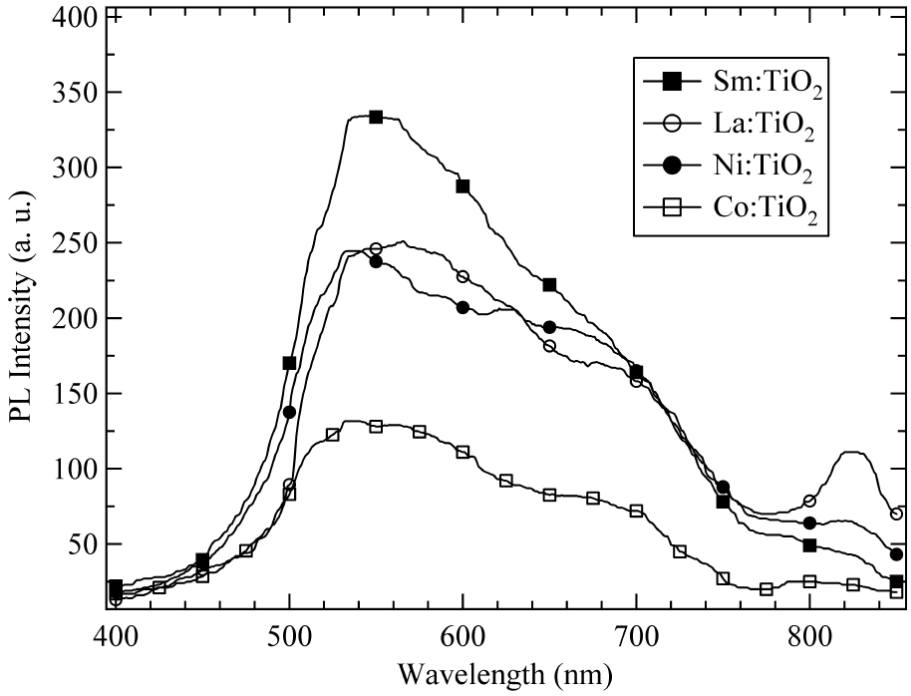

Figure 6. Photoluminescence emission spectra of thin films *M*:TiO_2/quartz, *M* = La, Sm, Ni, Co.

CONCLUSION

The thermal oxidation of two-layers structures $M/TiO_2/Si$(quartz) results in the compound oxide films formation. Doping metal determines the shift of short-wave transmission band edge and the optical transition energy. La and Sm doping shifts this edge to short-wave region and the edge wavelength equals 330 and 270 nm respectively. Ni and Co doping shifts this edge to long-wave region and the edge wavelength equals 355 and 370 nm respectively. The optical transition energy is equal to 3.70 and 3.06 eV and correspond to $La_2(TiO_3)_3$ and La_2TiO_5 respectively, 4.7 eV for Sm_2TiO_5, 3.64 eV for $NiTiO_3$ and 3.35 eV for $CoTiO_3$. The luminescence band of thin films M:TiO_2 is located in the region from 420 nm to 850 nm with maximum at 550 nm. Samarium doped titanium dioxide film has the most high intensity and complementary luminescence band with maximum at 830 nm.

ACKNOWLEDGMENT

This work supported by grant-in-aid under federal target program of Russian Federation: “Researches and elaborations in priority directions of development of a scientifically-technological complex of Russia for 2007-2012”, project No. 16.513.11.3008.

REFERENCES

[1] G.T.Crotty, P.J.Verlinden, M.Cudzinovic et al., 26th IEEE Photovoltaic Specialists Conference, Anaheim, CA, September 30 October 8, 1997, p. 1035.
[2] Y.Tonomura, H.Washio, K.Nakamura et al., 2nd World Conference and Exhibition on Photovoltaic Solar Energy Conversion, Vienna, Austria, July 6 10, 1998, p. 3511.
[3] H.K. Pulker, *Applied Optics*, 1969–1975 (1979) 12.
[4] Babuji, S. Radhakzishna, *J. Maiter. Sci Lett*. 767–769 (1985) 6.
[5] M. Graetzel, *Comments Inorg. Chem*. 12 (1991) 93.
[6] H. Takikawa, T. Matsui, T. Sakakibara, A. Bendavid, P.J. Martin, *Thin Solid Films* 145–151 (1999) 348.
[7] D.W. Hwang, H.G. Kim, J.S. Lee, J. Kim, W Li, S.H. Oh, *J. Phys. Chem*. B 2093-2102 (2005) 109.
[8] D.L. Wood, J. Tauc, *Phys. Rev*. B 3144 (1972) 8.

Smart Nanocomposites ISSN: 1949-4823
Volume 3, Number 1

STUDYING CORROSION PROTECTION WITH NANOSTRUCTURED POLYIMIDE COATINGS BY ELECTROCHEMICAL IMPEDANCE SPECTROSCOPY

Kirill L. Levine[1*], Van Fen, Natalia N. Nikonorova [2], Valentin M. Svetlichnyi[2], Vladimir E. Yudin[2], Ludmila A. Myagkova[2] and Nikolay S. Pshchelko[1]

[1] The St. Petersburg State Mining University.
Department of General and Technical Physics, St. Petersburg, Russia
[2] Institute of Macromolecular Compounds Russian Academy of Sciences,
St. Petersburg, Russia

ABSTRACT

In this study the anti-corrosion performance of polyimides modified with benzoquinone fragment was evaluated and compared with polyimide missing this fragment. The electrochemical impedance spectroscopy was employed to investigate polyimides pyropolymellitimide-oxydianiline (PMDA-ODA), polyimide-benzoquinone (PIQ), and polyamidoimide (PAI). The nano-effect discovered in earlier work was successfully confirmed: the impedance of nanostructured polyimides increased after the treatment with the corrosive solution before coatings failure. Therefore nanostructured systems can be utilized for "smart" corrosion protection.

Keywords: corrosion protection, polyimide, electrochemical impedance spectroscopy, nano-effect

INTRODUCTION

The development of nanotechnologies gives possibility to apply new principles to corrosion protection. One can think about a coating that responds to corrosive environment in "smart" manner: changes its properties under the influence of corrosive media. In this paper we observed an example of such a behavior: an attempt of a coating to recover its resistance to ions after some preliminary failure caused by the permeation of aggressive ions into the coating.

[*] Author to whom correspondence should be addressed. Email: levinkl@hotmail.com

Polyimides are used largely for microelectronics because of their excellent heat withstanding properties, chemical stability, and electrical resistance belonging to the range of excellent dielectrics [1].

These polymers appear to be attractive candidates for corrosion protection because of their good mechanical properties and high barrier properties [2]. Unfortunately, the majority of polyimides possess a strong tendency to absorb moisture that results in substrate corrosion [3]. In order to improve adhesion of polyimides to iron were suggested PIs with quinone functionalities [4, 5, 6] that have shown enhanced corrosion protection behavior. Introducing benzoquinone fragments into polyimide chain also improves thermal stability of this corrosion resistive coatings.

They are able to withstand short term heating up to 550^{o}C (in nitrogen) compared to 290^{o}C reported for "conventional" PI's [6]. Also the presence of benzoqiunone fragments improves adhesion to substrate.

The purpose of this study was to compare corrosion protection properties of different polyimides using method of Electrochemical Impedance Spectroscopy (EIS). Polymers selected for this study were: pyropolymellitimide-oxydianiline (PMDA-ODA), polyimide-benzoquinone (PIQ), and polyamidoimide (PAI) (Figure 1).

METHODS

Samples Preparation

PMDA-ODA (pyropolymellitimide oxydianiline) was obtained commercially under the trademark PM in the form of pre-polymer: poly(amic acid) (PAAc). Pre-polymer for PIQ was based on diamine AQMDA (X=CH_2); dianhydride ODPA (Y=O), (Figure 2). PIQ and PAI were synthesized at IMC RAS. PIQ was synthesized by a two-step polymerization of amine–quinone monomer (AQMDA) and aromatic dianhydride (ODPA) in 1-Methyl-2-pyrrolidinone (NMP), as shown in Figure 2. Similar procedure was applied to obtain PAI.

Thickness of polyimide films obtained by this procedure was 9-10 μm. All samples were heated at 300^{0}C to remove solvent and to complete the imidization.

Figure 3 shows schematic of electrochemical cell used in this experiment. Cylindrical cell was attached to a sample with mechanical clamp. It had 3 electrode configuration consisting of working electrode (film coated sample), Ag/AgCl reference electrode and counter electrode made from platinated grid. The cell was protected from electromagnetic interferences by Faraday cage. Steel panels of rectangular shape coated with different polymers were used for the experiments.

Cell was filled with 3% (mass) aqueous solution of sodium chloride. Electrochemical impedance spectra were recorded after different time of immersion of the sample into corrosive electrolyte. Experiment lasted 10 days. Measurements were taken in frequency range from 1 mHz to 5 kHz.

Potentiostat PC3 manufactured by Gamry was used for the experiments. Schematic of its connection to electrochemical cell is shown in Figure 4. Amplitude of applying signal at all measurements was 10 mV.

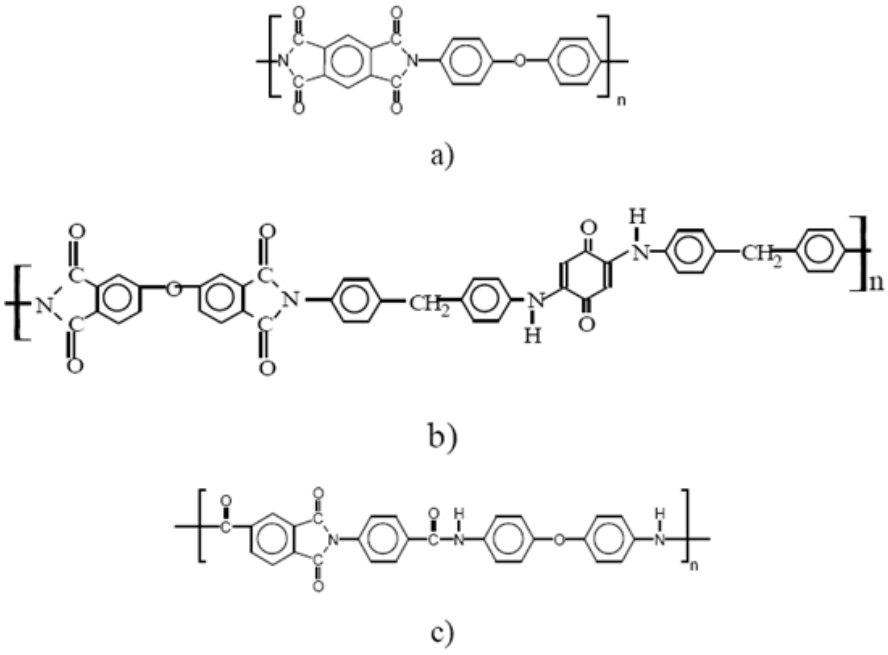

Figure 1. Chemical structures of polyimides used for corrosion protection. 1) Polyimide (PMDA-ODA); 2) Polyimide with quinone fragment (PIQ); 3) Polyamidoimide (PAI).

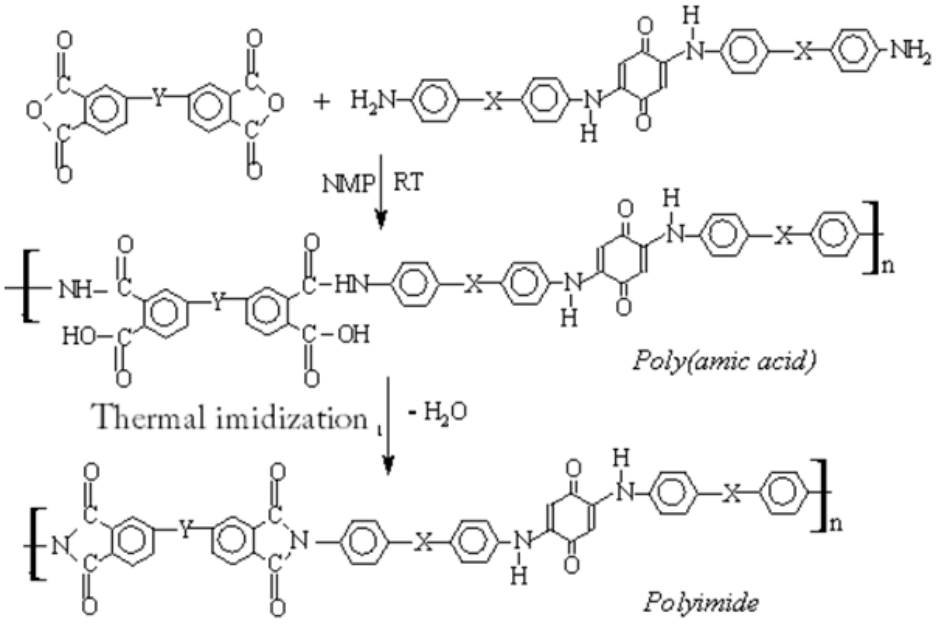

Figure 2. Two-stage synthesis of amino-quinone polyimide PIQ based on diamine AQMDA ($X=CH_2$) and dianhydride ODPA (Y=O).

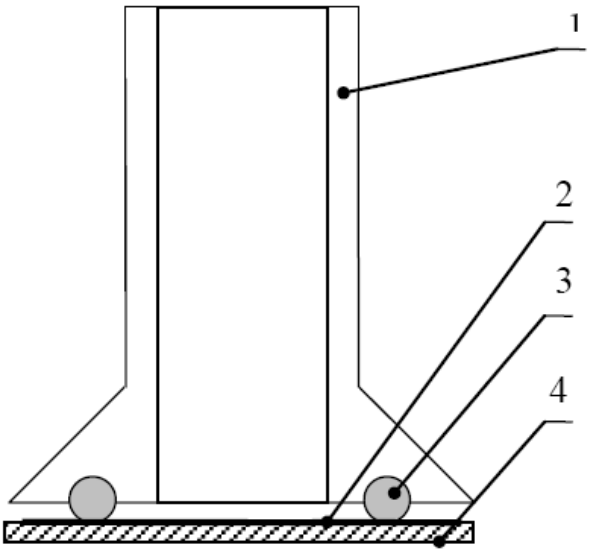

Figure 3. Schematic representation of electrochemical cell. 1 – glass part of a cell, 2 – sample, 3 – rubber ring, 4 – metal plate.

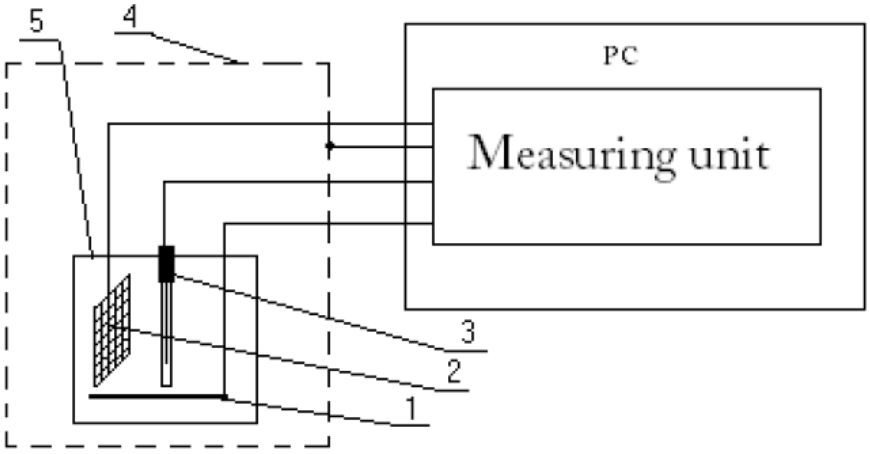

Figure 4. Apparatus used for the experiments. 1 Working electrode, 2 counter electrode, 3 reference electrode, 4 Faraday cage, 5 cell body.

RESULTS AND DISCUSSION

Figure 5 shows the appearance of PMDA-ODA, PIQ, and PAI samples after 167 h of immersion in corrosive media. Figures 6 - 8 show the impedance spectra of different coatings at different immersion times. Figure 9 presents the three-dimensional impedance plot made at 100 mHz for different samples at different immersion times.

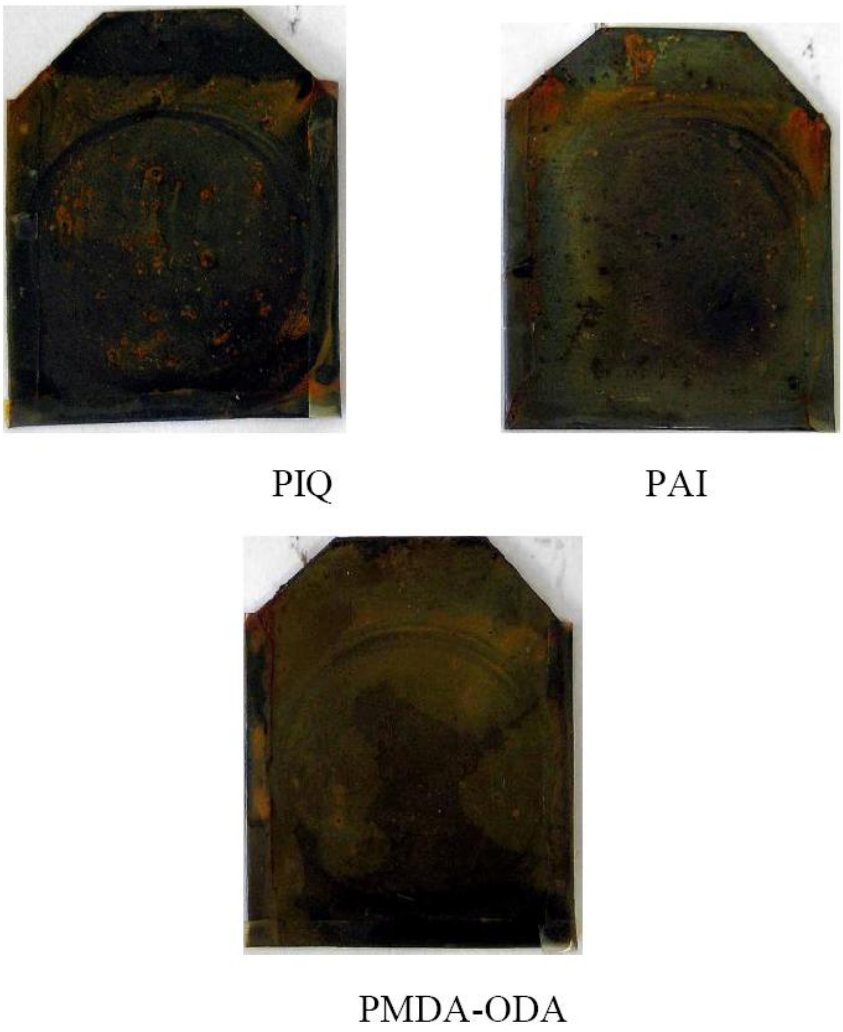

Figure 5. Photographs of samples after 167 h of immersion.

PMDA-ODA has shows "classical" behavior (Figure 6). It possessed relatively high impedance immediately after the immersion (>10^5 Ohm). After 215 h it failed by 2 orders of magnitude. Nyquist plot had shown the collapse of semicircle started at 167 h that meant the failure of barrier properties.

Bode plot of PIQ polyimide is shown in Figure 7. Even though the impedance initially possessed larger values than for PMDA-ODA polyimide (10^6 Ohm), it dropped to 10^3 after 167 h. This is worth notation that the impedance from $8.5 \cdot 10^2$ Ohm at 167 h shifted to $1.05 \cdot 10^3$ Ohm at 215 h (by (23±5)%) showing "non-classical" behavior.

Significant non-classical behavior was observed for PAI polyimide (Figure 8). Initial value of impedance of $1.1 \cdot 10^5$ Ohm dropped significantly to $6 \cdot 10^3$ Ohm at 167 h of immersion. However at 215 h it regained to $9 \cdot 10^3$ Ohm that is (50±10)% of the lowest value. This is worth of noting that in the case of PIQ polyimide the non-classical trend was observed within 0.1-10 Hz frequency range while for PAI polymer the trend was observed within the entire frequency range: from 0.1Hz to 5KHz.

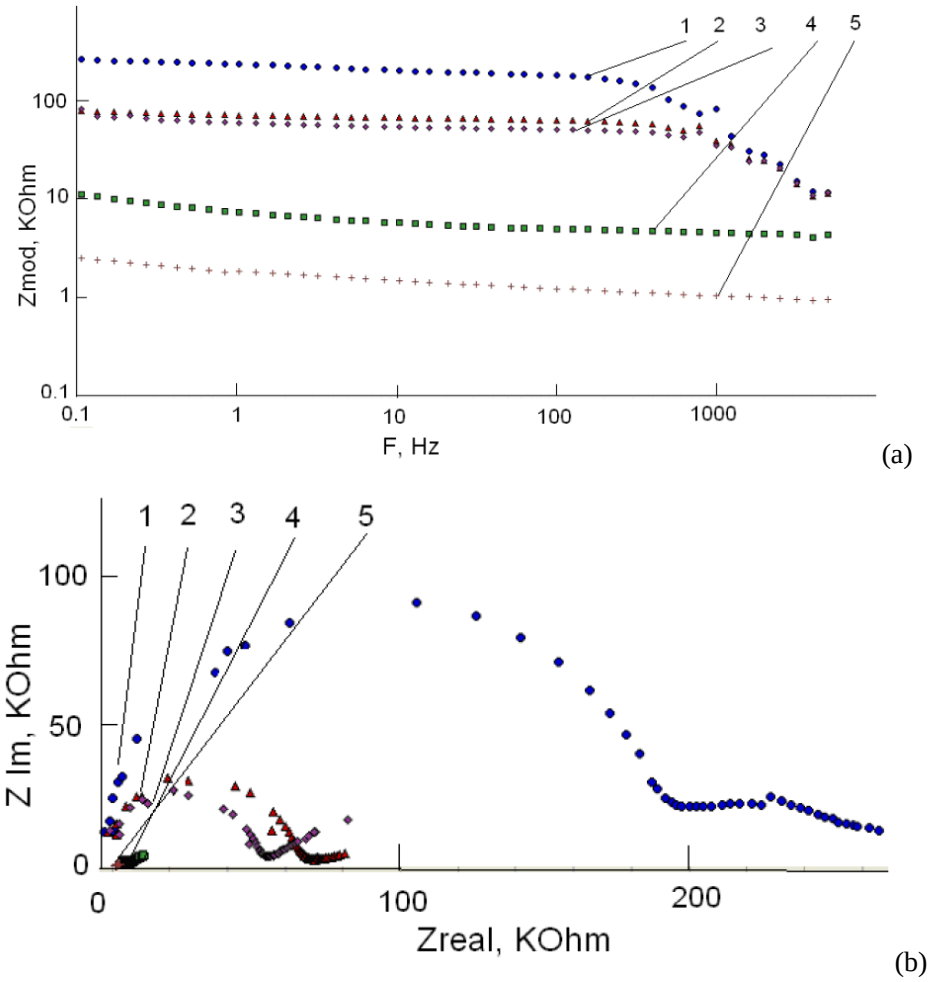

Figure 6. Electrochemical impedance spectroscopy of PMDA-ODA polyimide. (a) Bode plot, (b) Nyquist plot. 1 – 1 hour, 2 – 22 hours, 3 - 73 hours, 4 – 167 hours, 5 –215 hours.

3D plot of a coatings modulus is shown in Figure 9 reveals that PIQ possess the poorest corrosion protection properties while PAI and PMDA-ODA the best ones. At long-lasting forecast PIQ looks more promising than PMDA-ODA.

This interesting result can be attributed to a different type of response of PIQ polyimide to the ingress of aggressive ions into the coating and its swelling. Similar effect was reported in [7]. This effect was not observed for "classical" polyimide PMDA-ODA even though experiments were experiments were repeated few times. For PAI and PIQ the trend was repeatable. In PIQ and PAI the non-classical behavior possibly arises from the ability of molecular clusters to absorb moisture and to interrupt the diffusion through the mechanism of changed pore resistance [8] as a result of changing pore size [9].

Smart behavior of some polyimides is possibly related to the ability of their nanostructured morphology to adjust permeability to aggressive solution dynamically: change porosity as a result of swelling of nanostructured aggregates. More detailed close-look at the described effect will be performed in further investigation.

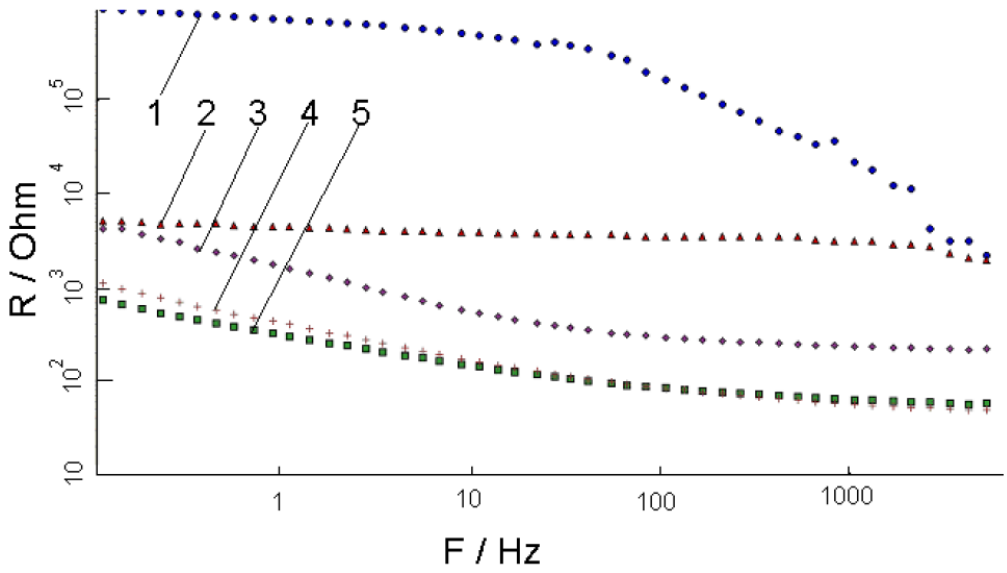

Figure 7. Bode plot of PIQ polyimide. 1 – 1 hour, 2 – 22 hours, 3 – 73 hours, 4 – 215 hours, 5 – 167 hours.

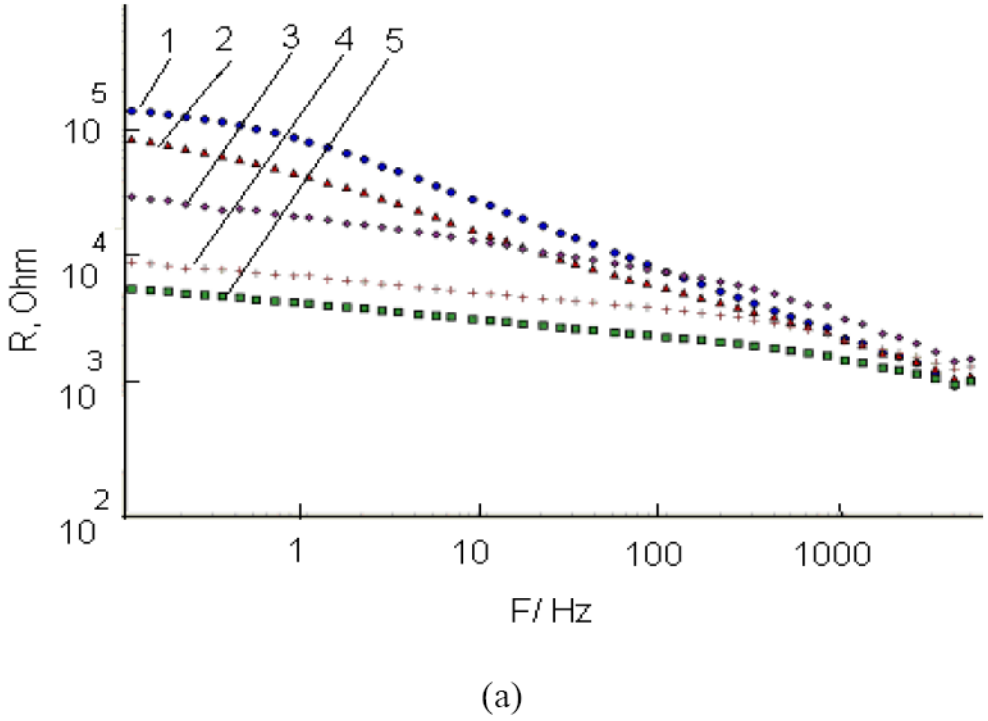

(a)

Figure 8. (Continued).

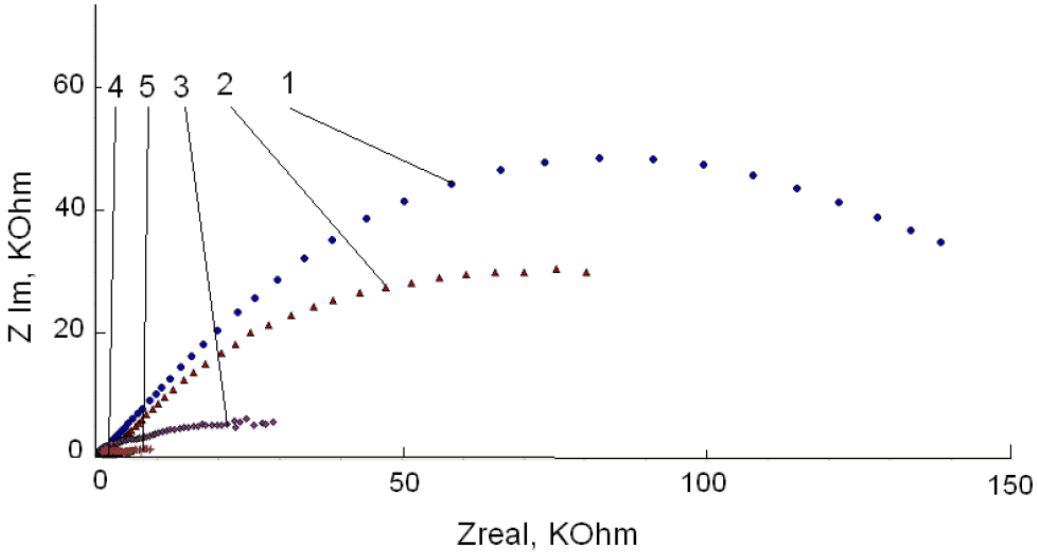

(b)

Figure 8. Electrochemical impedance spectroscopy of PAI polyimide. (a) Bode plot, (b) Nyquist plot. 1 – 1 hour, 2 – 22 hours, 3 - 73 hours, 4 – 215 hours, 5 – 167 hours.

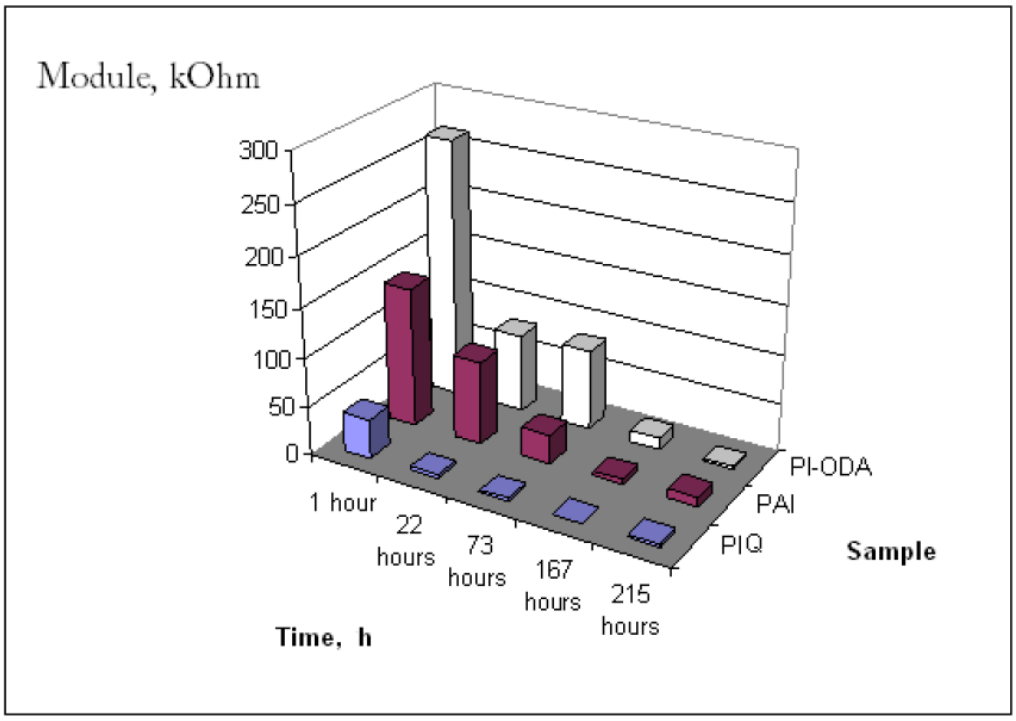

Figure 9. Impedance data for different samples at 100 mHz at different immersion times.

CONCLUSION

The comparison of PAI, PIQ and PMDA-ODA polyimides have revealed that these 3 different polymers possess different corrosion protective properties, show different response to corrosion. It was determined that PIQ and PAI polyimides show "nano-effect". After certain time of immersion their impedance increases quite significantly possibly due to the swelling of nanostructures under the ingress of corrosive liquid. Therefore, further investigation of PAI and PIQ with nano-additives will be promising from the point of view of using nanostructured materials as smart coatings for corrosion protection.

ACKNOWLEDGMENTS

Acknowledgements are brought to colleges from the Institute of Macromolecular Compounds Russian Academy of Science: Vladimir E. Yudin, Valentin M. Svetlichnyi, and Ludmila A. Myagkova for preparation of nanostructured samples.

REFERENCES

[1] Bessonov, M.M.Koton, V.V. Kudryavtsev, L.A. Laius. Polyimides-Thermally Stable Polymers, *Plenum Publishing Corp.*, New York, 1987.

[2] Sazanov Yu. N. Applied Significance of Polyimides, *Russian Journal of Applied Chemistry*, 2001, v. 74, No 8, p. 1266.

[3] Tan, E. K.; Bellucci, F.; Kloppers, M. J.; Latanision, R. M., *Mater Sci Forum* 1992, 111–112, 177–190.

[4] Kaleem, K.; Chertok, F.; Erhan, S. *Prog. Organ. Coat* 1987, 15, 63–71.

[5] Nithianandam, V. S.; Chertok, F.; Erhan, S., *J. Coat. Technol* 1991, 63, 47–49.

[6] Han N. M., Bie H., Nikles D.E.,Warren G.W., *Corrosion Journal of Polymer Science: Part A: Polymer Chemistry,* Vol. 38, 2893–2899 (2000).

[7] Tallman D.E., Levine K.L,Siripirom Ch, Gelling V.J., Bierwagen J.P., and Croll S.G., *Applied Surface Science*, 254 (2008) 5452 – 5459.

[8] Levine K.L. and Iroh J.O. "Resistance of the Polypyrrole/Polyimide composite by electrochemical impedance spectroscopy", *Journal of Porous Materials*, 11, (2004), 87-95.

[9] Levine K.L., Pshchelko N.S., Electrochemical Properties of a Polypyrrole-Polyimide Composite, *Polymer Science series A (Polymer Physics)*, 2011, Vol. 53, N 6, p 510-520.

Smart Nanocomposites ISSN: 1949-4823
Volume 3, Number 1

SURFACE-NANOSTRUCTURED METALS AND THEIR TRIBOCHEMICAL PROPERTIES

A. G. Syrkov*

Saint-Petersburg State Mining University, St. Petersburg, Russia
Scientific-educative Center of Nanotechnologies, St. Petersburg, Russia

ABSTRACT

The possibilities of the adsorption modification of the surface of metal powders in vapors of quaternary ammonium compounds for regulation of the tribochemical properties of metals and lubricants containing these metals as additives was analyzed. The general trend is that in order to achieve a minimal index of friction (D) of tribological pair with a lubricant, a combination of few properties of compounds is necessary. One is good water-repellent, and another is low reactivity. It was revealed that solid-state synthesis of metals in vapor of hydrophobic silicone liquid based on organohydridesiloxanes is perspective for obtaining Si-C-containing surface-nanostructured metallic composites (M = Ni, Cu, Fe) with high temperature stability. The mechanism of this synthesis, according to XPS and other techniques, allows to regulate with precision the structural and chemical characteristics of metallic materials, including values of electron energy in the Si2p surface layer level in the range 102-106 eV. Maximum of high temperature stability in air has a sample on the basis of iron.

Keywords: adsorption modification, solid-state hydride synthesis of metals, metal powders, nanostructured metallic composites

INTRODUCTION

The problems of stability properties of metals and improvement the quality of metals are important not only in their preparation, but also in the process of storage and functional use. The urgency of these challenges in the XXI century is increased in connection with the demand of industry in dispersed and nanostructured metallic materials. Disadvantage of latter, as a rule, is low stability in air and in aggressive technogenic environments. Metals as thin film and a highly dispersed belong to the class of metal-dielectric structures and metal-dielectric-semiconductors (MDS), which are the basis for many intelligent electronic devices. In

* E-mail: syrkovandrey@mail.ru

addition, nanostructured metal powders are used for filling and properties improvement of various organopolymer compositions [1,2].

Most of being developed today nanotechnology methods of metals are often quite expensive and energy consuming (electrical explosion, synthesis in plasma, plastic deformation of metals). The main thing - they do not solve the central problem of modern solid-state production: to provide reliable reproducibility of structure and properties of materials from one sample to another and from synthesis to synthesis.

In some cases quite successful and proven can be approach that is based on the irreversible chemisorption in terms of various substances on the surface of dispersed or compact metals [2,3]. In this case, it will be more accurate to talk about getting not just a nanostructured materials (nanocomposites) but the synthesis of surface-nanostructured metals [2]. In the most general case, the metal-substrate does not need to be a nanostructured material, and may represent a roughly dispersed metal powder or, for example, conventional steel [4,5]. Many of metals applications (adsorption, catalysis, lubrication, friction and electronics) impose sufficiently high requirements to the surface material properties including its thermal and chemical stability. Therefore, it seems logical to apply nanotechnology methods that will lead primarily to improved quality of metal surface.

In this paper some particular qualities of tribochemical properties of surface-nanostructured metals (Al, Cu, Ni, Fe), obtained by solid-state hydride synthesis and the adsorption modification of metals by cationic tensides based on quaternary ammonium compounds are considered. The above methods of synthesis and surface modification of metals were developed under the guidance of the author [2, 4-8, 9].

Solid-state hydride synthesis of metal materials is a reduction in an open flow system under the specified program of solid metal compounds by thermally stable volatile elementohydride compounds (NH_3, CH_4, SiH_4, CH_3SiHCl_2, etc). This method is based on laid out solid metal halides and oxides (Ni, Fe, Cu, Zn) reduction by heating. By this method we have produced metals and new surface-nanostructured dispersed metallic materials [2,4,6]. Conditions of synthesis guarantee that the adsorption of reducing agent on metal do not exceed the value of monolayer adsorption. From the measured XP-spectra of samples it follows that adsorbed elementohydride chemically interacts with the reduced metal, i.e. reductant's molecules are chemisorbed [2,4]. The peculiarity of our proposed method is that depending on the selection of a reducing agent, direct control of the specific surface of solid material, its thermal and chemical stability, electron binding energy of the characteristic level of surface atoms (XPS data) is possible [4 ,6]. Of particular interest is the reduction of metals in vapor of methyldichlorosilane (CH_3SiHCl_2) or organohydridesiloxanes with subsequent heat treatment in a flow of methane (natural gas). As a result of this synthesis metallocomposites are formed with Si-C-containing protective surface nanofilm, which gives metal a unique heat resistance, good water-repellent and organophilic properties [2, 8].

I. Surface-Nanostructured Metals Obtained by Method of Adsorption Modification and Their Properties

For surface treatment of metals from aqueous solution and vapor phase we used alcamon (A) and triamon (T) as a substance-modifiers, which in Russia are traditionally used to impart

antistatic properties to the textile and polymer materials. The composition of T corresponds to the chemical formula $[(HOC_2H_4)_3N^+CH_3][CH_3SO_3^-]$. Alkyl radical in alcamon's cation corresponds to the number of carbon atoms n = 10 ÷ 18. The original aluminum powder (specific surface 2,6 m^2/g), copper (0,6 m^2/g) and carbonyl nickel (0,4 m^2/g) were treated in A and T vapor [2]. Metals were treated with either one preparation (A or T) or a mixture of (A + T) or sequential interaction of metal (M) with T and A. We have obtained a series of samples, respectively, of the form: M/A, M/T, M/(A + T), M/T/A, where M = Al, Ni, Cu. In addition, as a sample of comparison we used the powder form M/HSL. This powder is dispersed metal treated by vapor of hydrophobic silicone-organic liquid (HSL). The magnitude of adsorption of water vapor (aH_2O) was measured by the dessicator method under P/P_0 = 0,96-0,98 (20 ± 2^0C). Reactivity determined gravimetrically by measuring specific weight gain during the oxidation of samples in a furnace (1113 K, 300s) in the free access of air (P = 1 atm, humidity is 60 ± 10%). The antifriction properties of powders were evaluated by acoustic emission method. Integral index D (proportional to the friction force) in the tribological pair drill - a steel plate with a lubricant that contains a metal powder was studied [2]. D was measured on a special stand in the ultrasonic range of frequencies (20-300 kHz) with the help of a certified device ARP-11. The content of the powder additives in the lubricant was 0,5-1,0 mass%.

The analysis of three-dimensional relationships between integral friction index D and reactivity and the magnitude of adsorption of water vapor is shown in Figures (1-3) and Tables (1-3). Dependencies are 3dimentions space curves that reflect the influence of surface modification of metal on the antifriction properties of lubricant under boundary friction. The simplest dependence we have for the lubricant filled with Al- or Ni-samples. There is a general trend: D decreases (friction decreases) with decreasing reactivity of the filling powders (Figures 1-4). In the case of powders based on aluminum it is observed that D decreases, as a rule, with decreasing values of aH_2O (i.e. with increasing hydrophobicity of the samples), as shown in Table 1.

Table 1. Values of and aH_2O for Al-samples

Filling powder	aH_2O, %	D for industrial oil (I-20) with powder (p=47 MPa)
Al/T	0.17	780
Al/A	0.22	910
Al/ (A+T)	0.13	300
Al	0.23	1690
Al/T/A	0.16	1000

For convenience of comparison with the data of Figures (1-3) the composition of powder samples in Tables (1-3) is shown by the increase in their reactivity (for example, from Al/T to Al/T/A, Table 1).

From Tables 1 and 2 we can see that the powder M/(A + T) has the stronger effect on friction reduction than the powder form M/A and M/T (M=Al,Ni).

For lubricant with the addition of Al/(A + T) D value is the smallest: 300, for lubricants with additives Al/A and Al/T respectively, D is equal to 910 and D is equal to 780 (Table 1), respectively .

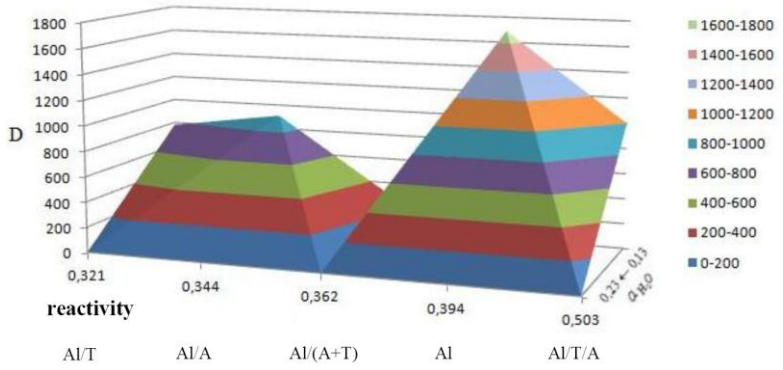

Figure 1. Diagram of D relationship with the value of adsorption of water vapor and the reactivity during the oxidation of the modified metal additive on the basis of Al-powder.

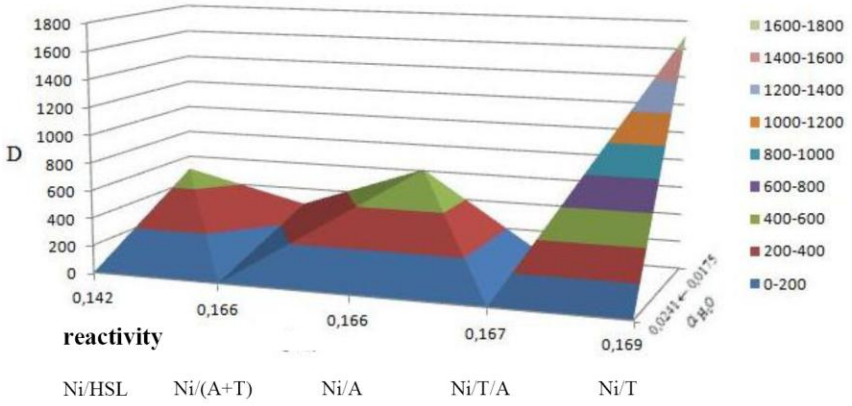

Figure 2. Diagram of D relationship with the magnitude of adsorption of water vapor and the reactivity during the oxidation of the modified metal additive on the basis of carbonyl nickel.

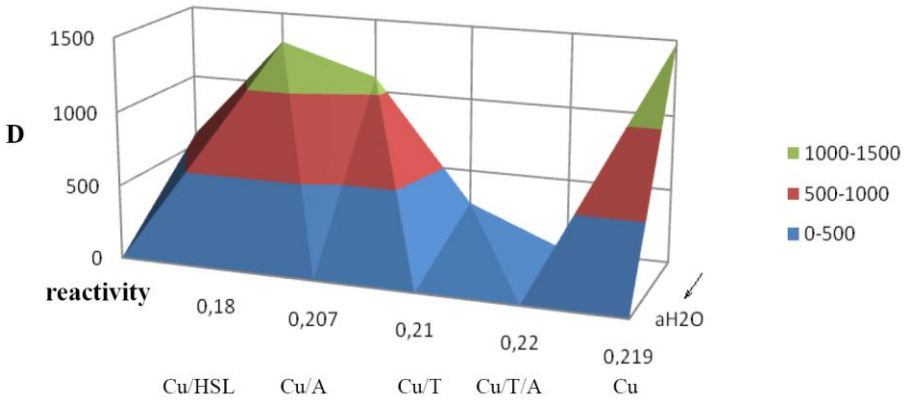

Figure 3. Diagram of D relationship with the magnitude of adsorption of water vapor and the reactivity during the oxidation of the modified metal additive on the basis of copper powder (PM1).

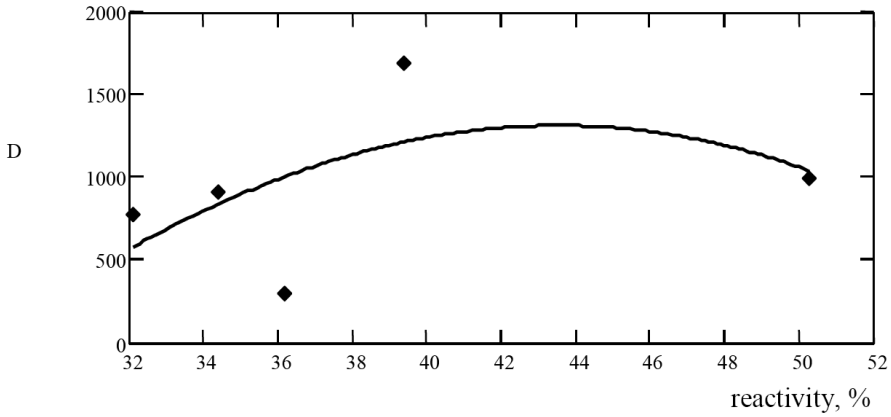

Figure 4. Dependence of D from filler reactivity for lubricant with additives on Al-base. Approximation equation (Math Cad) is $D=7.11y-7.03y^2-4330\ln y$, where y=reactivity.

Table 2. Values of D and a_{H2O} for Ni-samples

Filling powder	a_{H2O}	D for industrial oil with powder
Ni/ HSL	0.0175	500
Ni/ (A+T)	0.0212	280
Ni/ A	0.0212	610
Ni/T/A	0.0205	-
Ni/T	0.0191	1700 (dry friction)
Ni	0.0241	280

In fact the influence of A and T is synergistic. They act in a manner that the activity of their mixture (A + T) to D exceeds the activity of individual components.

Dependence of D on the reactivity and aH_2O, as can be seen from Table 3, for Cu-samples is more complicated. The synergistic effect on D was observed in the powder consistently treated by T and A (Cu/T/A). On the sample treated by a mixture of modifiers (A + T), in contrast to the Al/(A + T) and Ni/(A + T), a marked increase in D (Table 3) until 1480 takes place.

Table 3. Values of D and a_{H2O} for Cu-samples

Filling powder	a_{H2O}	D for industrial oil with powder
Cu/HSL	0.0205	580
Cu/A	0.0299	1300
Cu/T	0.0268	1100
Cu/T/A	0.0260	270
Cu	0.0445	-
Cu/(A+T)	0.0310	1480

The friction in the system increases. The general trend, which is observed for all modified metallic additives on the basis of Al, Ni, Cu is the following. To achieve the minimum D

(lowest friction) in the tribological pair with a lubricant, combination of good water reppelent properties and low reactivity of the additives is favorable. A clear illustrations of this rule are the properties of additive Al/(A + T) in Table 1, Ni/(A + T) in Table 2 and Cu/T/A in Table 3. The reactivity of these additives as is evident from these Tables and Figures 1 – 4 has a sufficiently low level (Ni/(A + T)), or less than the average level of this properties in a series of modified samples on the basis of the corresponding metal (look samples Al/(A + T) and Cu/T/A).

The synergistic effect of D for the latter sample can be explained in the following way. According to modern concepts, in order to achieve the maximum of antifriction effect for solid surfaces treated with surfactants, it is necessary to combine high hydrophobicity of the surface and good adhesion of deposited films to the original surface [2]. Data of our studies testify that from two of these factors, the latter factor (adhesion) is the most important [9]. Metal processing by two types of surface-active substances (A and T), in general, is favorable to the implementation of both significant factors. T molecule with nitrogen atom that contains small organic radicals, interacts with metal surface. This interaction, according to XPS, is possible due to donor-acceptor bond with the transfer of electrons from N to M [2, 4, 9]. Due to this bond, it is obvious that there is a stabilization (increased adhesion) bilayer film T / A on metal surface after consistent treatment with mentioned modifiers, which have structural compliance, as both are quaternary ammonium compounds (QAC). Ensuring good adhesion of the film T / A under similar treatment of aluminum and nickel is difficult because their initial surface contains organic impurities [2]. Used Al-powder (trade-mark PAP-2) has a stearin nanofilm on its pre-coated by the factory. Selected for the experiments carbonyl nickel powder (PNK-UT3) is also characterized by a high content of carbon (carboxyl groups) in its surface layer.

In terms of the boundary and dry friction at high load pressures when the liquid lubricant (oil) is squeezed out of zone of tribological contact drill-plate, the measured friction index D to a large extent is determined by the antifriction properties of solid surfaces metallic additives [2]. This obviously explains the fact that the minimum of D for lubricant with copper additives is observed on the powder type Cu / T / A (Table 3). When using additives based on Al-powder the lubricant with sample Al / (A + T) has the lowest D . The advantage of processing additive mixtures, is apparently due to the fact that the heteroatomic interaction of triamon and metal according to scheme N → M is hindered because of stearin films on aluminum. Triamon-alcamon film can better stabilize the surface of the additive due to structural similarity of hydrocarbon radicals of alcamon and stearin [2,4].

II. Solid-State Synthesis of Si-C-Containing Metallic Powders and Their High Temperature Stability

Reduction vapor of HSL based on organohydridesiloxanes on the first stage was recently used for obtaining surface-nanostructured SiC-containing metal powders [2]. The advantage of HSL over methyldichlorsilane applied earlier [4,8] is that HSL is less toxic. Treatment on the second stage of the synthesis in methane is still necessary because it allows to reduce metal contents in the volume of solid phase, where penetration of large molecules HSL is difficult enough. After the reduction of solid metal oxides (MO) or chlorides (MCl_2), obtained metal powders have properties and characteristics presented in Table 4.

Table 4. Structure-chemical characteristics of Si-C-containing metal powders

Sample, way of obtaining	Specific surface, m^2/g	Δm for 100 h (900^0C) on air, mcg/cm^2	Atomic ratio M/Si in surface layer (XPS)	E_{Si2p}, eV	Chemical shift for $M2_{p3/2}$-level, eV
$NiCl_2$+HSL+CH_4	10	0.398	0	104.7	2.5
NiO+HSL+CH_4	61	0.395	0	105.6	1.4
CuO+HSL+CH_4	13	0.301	0.9	103.8	2.6
FeO+HSL+CH_4	2	0.102	1.1	102.5	5.0

Mass increase (Δm) of metal powders during oxidation is at the level of 0,1-0,4 mcg/cm^2, that is in 17 - 70 times lower than Δm for hot-resistant nikel-chrom alloys (about 7 mcg/cm^2). The samples have high hot stability, which is regulated depending on the type of metal. Synthesis also allows to adjust the surface area of powder and binding energy of electrons (oxidation) of the surface atoms of Si (Table 4). The sample most chemically stable during high temperature oxidation on Fe base possessed the lowest binding energy of Si2p characteristic level (102 eV) for silicon in the Si-C-groups of the modifying metal, and the maximum level of the chemical shift M2p3/2 of the relevant metal. According to our ideas [2,4,8], it can be interpreted as follows. Metallic iron, as the most chemically active metal, compared with Ni and Cu, most willingly gives up its electrons to the vacant 2p orbitals of silicon. Thus there is a sufficiently strong heteroatomic M → Si interaction between the metal and the protective Si-C-containing (carbosiloxane) film. Iron, in fact, passivated. The corresponding sample therefore has a maximum temperature stability (minimum Δm), which is confirmed experimentally (Table 4). The synthesized powders were studied in details by IR-spectroscopy, RFA, XRD. In particular, transmission electron microscopy has shown that the thickness of the protective Si-C-containing film on the metal was less than 5 nm [2,9].

CONCLUSION

The possibilities of the surface adsorption modification method of metal in vapor of cationic tenside preparation (triamon and alcamon) with very different-sized hydrocarbon radicals on the nitrogen atom are reviewed. There are established routes of strengthening of hydrophobicity, and reactivity of surface-nanostructured metals depending on the program of modifying of powders. A general trend of changing of the integral index of friction D for a tribological pair with a lubricant containing various powders modified metals was identified. To achieve the minimum D (lowest friction) favorable combination of good water repellent surface properties and low reactivity of metal powders is needed. Synergistic effects of antifriction properties of lubricants which were observed when using the Al, Ni, Cu based powders additives were detected and interpreted. Found relationships (D-adsorption of water vapor - the reactivity of the powder) are of interest for the selection of perspective antifriction additives on the basis of ductile metals for industrial oils. Based on these results are simple gravimetric measurements of adsorption properties and reactivity of dispersed metallic additives.

Solid-state hydride metal synthesis in HSL vapors of is promising for the creation of new surface-nanostructured Si-C-containing metal-composites with unique temperature stability. The mechanism of the synthesis, according to XPS and other techniques, allows the fine regulation of the structural and chemical characteristics of the obtained metallic materials based on Ni, Cu, Fe. Maximum temperature stability in air (Δm = 0,1 mcg/cm^2 under 900^{0}C, 100 h) was shown by a sample on the basis of iron.

ACKNOWLEDGMENTS

The author would like to thank post-graduate student L. Yachmenova for help in getting up of article materials.

The work was supported by Analytical Department Program «Development of scientific potential of high school» (2009-2011) of Ministry of education and science RF, project № 1.13.08, № state reg. 0120.0852107.

REFERENCES

[1] S.Thomas, G.Zaikov, S.Calsaraj, A.Meere, Recent Advances in Polymer Nanocomposites: Synthesis and Characterisation, *CPI Antony Rowe*, (2010).

[2] I.N.Beloglazov, A.G.Syrkov, Chemicophysical bases and methods of obtaining of surfacely-nanostructured metals, *St.Petersburg State University*, (2011).

[3] V.B.Aleskovsky, Stehiometry and synthesis of solid compounds, Nauka, (1976).

[4] A.G.Syrkov Methods of Physics and Chemistry in Obtaining of Nanostructured Metals and in Nanotribology, Non-ferrous Metals. *Nano-Structured Metals and Materials*, 4, (2006), 10-15.

[5] I.Pleskunov, A.Syrkov, D.Bystrov, On uniform principles and ways of creation of nanostructured metallic and antifrictional materials on steel base, *CIS Iron and Steel Review*, 1-2, (2008), 23-25.

[6] A.Syrkov, Hydride solid state synthesis of dispersed metal and metal-ceramic materials with chemical stability, *Proc. Int. Symp. on Reactivity of Solids*, (1996), 31-33.

[7] I.Yartsev, I.Pleskunov, A.Syrkov, D.Bystrov, Interrelation of water-repellent and protective properties of coatings on steel and role of nanostructured additives, *CIS Iron and Steel Review*, 1-2, (2008), 26-29.

[8] A.Syrkov, L.Mahova, Hydride synthesis of SiC-containing metallic composite materials, *Proc. of Int.Conf. on Electronic Ceramics – Production and Properties*, (1990), 113-115.

[9] N.S. Pshchelko, A.G. Syrkov, T.G. Vahreneva et. al., Electrophysical and chemico-physical micro- and nanotechnology of adhesion's enhance of the components in the metal- dielectric system, *Russian Nanotechnologies*, 11-12, (2009), 42-47.